J. Nonlinear Sci. Vol. 14: pp. 119–171 (2004)
DOI: 10.1007/s00332-004-0568-2

Journal of
Nonlinear
Science



# Energy Minimization and Flux Domain Structure in the Intermediate State of a Type-I Superconductor

R. Choksi,[1] R. V. Kohn,[2] and F. Otto[3]

[1] Department of Mathematics, Simon Fraser University, Burnaby, BC V5A 1S6, Canada
e-mail: choksi@math.sfu.ca

[2] Courant Institute, New York University, New York, NY 10012, USA
e-mail: kohn@cims.nyu.edu

[3] Angewandte Mathematik, Universität Bonn, 53115 Bonn, Germany
e-mail: otto@iam.uni-bonn.de

Received February 5, 2003; accepted December 15, 2003
Online publication April 7, 2004
Communicated by A. Mielke

**Summary.** The intermediate state of a type-I superconductor involves a fine-scale mixture of normal and superconducting domains. We take the viewpoint, due to Landau, that the realizable domain patterns are (local) minima of a nonconvex variational problem. We examine the scaling law of the minimum energy and the qualitative properties of domain patterns achieving that law. Our analysis is restricted to the simplest possible case: a superconducting plate in a transverse magnetic field. Our methods include explicit geometric constructions leading to upper bounds and ansatz-free inequalities leading to lower bounds. The problem is unexpectedly rich when the applied field is near-zero or near-critical. In these regimes there are two small parameters, and the ground state patterns depend on the relation between them.

***Contents***

## 1. Introduction

The intermediate state of a type-I superconductor is induced by an applied magnetic field of suitable magnitude. In this state, the material forms a microscopic mixture of normal and superconducting domains. A model based on energy minimization was introduced by Landau in 1937 [33]; it was among the earliest "Landau theories" of condensed matter physics. A rich theoretical and experimental literature had developed by the 1970s—reviews can be found in the 1969 article by Livingston and DeSorbo [37] and the 1979 book by Huebener [23]. The subject was dormant for many years, but has recently begun to attract fresh attention [15], [19], [40].

This paper pursues a theme begun by Landau and revisited by many others since. We examine the scaling law of the minimum energy and the qualitative properties of domain patterns achieving this law. Our motivation is not that the system actually minimizes its energy. Indeed, the details of the intermediate state are highly history-dependent, with many metastable states. However the observable structures should have relatively low energies. One therefore expects them to share the energy scaling of the ground state.

As we shall explain in Sections 2 and 3, the minimum energy has the form

$$E = E_0 + E_1, \tag{1.1}$$

where $E_0$ is the value obtained by ignoring surface energy and $E_1$ is the correction due to nonzero surface tension. The scaling law of interest is the dependence of $E_1$ on the surface tension $\varepsilon$ of the normal-superconductor interface and the normalized magnitude $0 < b_a < 1$ of the applied magnetic field.

The leading order term $E_0$ was completely understood by Landau. It describes the limiting behavior as the surface tension $\varepsilon \to 0$. This corresponds to a "thermodynamic" theory of the intermediate state, determining e.g. the volume fraction of the normal domains. Mathematically, it is associated with the *relaxation* of the underlying nonconvex variational problem.

To study domain structure, however, one must look beyond relaxation to the principal-order correction $E_1$. Our goal is therefore (i) to identify the scaling law of this correction, and (ii) to understand what microstructural features are required to achieve this scaling law. Our analysis is restricted to the simplest possible case: a plate of thickness $L$ under a transverse applied field.

There are a number of different regimes, each associated with a different microstructural picture. Here is an informal summary (these results will be developed more gradually, and stated more carefully, in Section 3):

(a) For intermediate values of $b_a$, bounded away from 0 and 1, $E_1 \sim \varepsilon^{2/3} L^{1/3}$. It is relatively easy for a flux domain pattern to achieve this law; the main requirement is that its local length scale be about right.

(b) For relatively small values of $b_a$, in the range $(\varepsilon/L)^{2/7} \lesssim b_a \ll 1$, the prefactor is proportional to $b_a^{2/3}$. Thus $E_1 \sim b_a^{2/3} \varepsilon^{2/3} L^{1/3}$; to achieve this scaling the magnetic flux should cross the sample by a uniformly distributed family of branched flux tubes.

(c) For the smallest values of $b_a$, when $b_a \lesssim (\varepsilon/L)^{2/7} \ll 1$, the scaling law is different. Indeed, in this regime $E_1 \lesssim b_a \varepsilon^{4/7} L^{3/7}$. Notice that this is smaller than the scaling law of (b), since $b_a \varepsilon^{4/7} L^{3/7} \ll b_a^{2/3} \varepsilon^{2/3} L^{1/3}$ when $b_a \ll (\varepsilon/L)^{2/7} \ll 1$. To achieve this scaling the magnetic flux should cross the sample by a nonuniformly distributed family of branched flux tubes.

(d) For relatively large values of $b_a$, i.e. for $b_a$ near 1, the situation is similar to (b), but not quite the same. The prefactor is proportional to $(1 - b_a)$ with a logarithmic factor: $E_1 \lesssim (1 - b_a)|\log(1 - b_a)|^{1/3} \varepsilon^{2/3} L^{1/3}$. To achieve this scaling (with the logarithmic factor) the magnetic flux should fill most of the sample, leaving a uniformly distributed family of superconducting tunnels.

(e) For the largest values of $b_a$, the sample is entirely normal and $E_1 \sim (1 - b_a)^2 L$. This is preferred when $(1 - b_a)^2 L \ll (1 - b_a)|\log(1 - b_a)|^{1/3} \varepsilon^{2/3} L^{1/3}$, i.e. when $(\varepsilon/L)^{2/3} \gg (1 - b_a)|\log(1 - b_a)|^{-1/3}$.

The optimality of the scalings described in (c) to (e) is not proved in this paper; rather, we shall address this in [12]. But we do prove here that (d) is optimal up to the logarithmic factor, i.e. $E_1 \gtrsim (1 - b_a) \varepsilon^{2/3} L^{1/3}$.

Notice that the problem is richest when $b_a$ is near 0 or 1. This is natural. For intermediate values of $b_a$ there is just one small parameter, $\varepsilon/L$, but for extreme values of $b_a$ there are *two* small parameters. So it is quite reasonable that the energy-minimizing behavior should depend on the relation between them.

Landau's variational description of the intermediate state is basically a nonconvex variational problem regularized by surface energy. Such problems arise in many areas of

condensed matter physics. They have recently attracted a lot of attention as examples of energy-driven pattern formation. Thus our work is conceptually close to recent studies of martensitic phase transformation [13], [28], [29], [30], micromagnetics [10], [11], compressed thin film blisters [3], [26], and block copolymers [9], [38], [41]. However most of these references address problems with a single small parameter: the normalized surface tension. The present paper is different, due to our interest in extreme applied fields (near-zero and near-critical $b_a$)—where the problem has two small parameters.

There is nothing particularly new about the idea of using energy minimization to understand the intermediate state. We review the relevant literature in Section 2. But briefly: past investigations have generally minimized the energy within specific, relatively simple classes of patterns. The weakness of this approach is obvious: minimization within a restricted class gives only an *upper bound*. Proving it is a good bound—showing the restricted class was chosen well—requires a matching, ansatz-independent *lower bound*.

Our work is different: we provide lower as well as upper bounds. This is, to our knowledge, the first treatment of ansatz-free lower bounds for the energy of the intermediate state. We actually develop two rather different approaches. One uses a sort of "dual problem" to estimate the magnetic energy between two cross-sections (Section 5). The other takes advantage of an analogy to micromagnetics, and recent progress in that setting (Section 7).

The need for a more global, ansatz-independent understanding has long been recognized by theorists. For example, in 1957 Balashova and Sharvin wrote: "In one way or another all the formulas proposed for connecting the surface tension with the dimensions of the domains have been obtained only under various simplifying assumptions, still requiring experimental verification, about the shapes of the domains" [2]. This statement, written over 45 years ago, remains equally valid today. Our analysis avoids the simplifying assumptions criticized by Balashova and Sharvin, by considering lower as well as upper bounds.

One might have expected that after 65 years of study, the list of possible regimes would long since have been identified. Actually, it was not. Of the regimes (a)–(e) listed above, only (a), (b), and (e) have been recognized in the literature. The constructions associated with (c) and (d) are (to the best of our knowledge) new. Even the observation that for $b_a$ near 0 or 1 there are two small parameters, and that the relation between them should matter, appears to be new.

Our analysis provides insight concerning several aspects of the intermediate state:

(i) *Hysteresis.* Flux patterns created by increasing the applied field from 0 are very different from those generated by decreasing it from the critical field. This is consistent with the fact that the constructions associated with regimes (b), (c), and (d) are rather constrained and quite different from one another. Structures nucleated when $b_a$ is near 0 tend to persist as the field increases, because for intermediate values of $b_a$ the cross-sectional geometry doesn't really matter.

(ii) *In-plane complexity.* The domain patterns seen experimentally are typically quite complex, particularly for intermediate applied fields (well away from $b_a = 0$ or 1). It is natural to ask whether such complexity is energetically favored. The answer is no, at least at the level of the scaling law. Indeed, our lower bounds show that

no pattern, regardless of its complexity, can achieve a better scaling law than the simplest ordered constructions.

(iii) *Varying length scale.* Landau was the first to suggest that for $\varepsilon/L \ll 1$ the length scale of the microstructure should vary with depth. Our lower bound confirms this, by showing that if the microstructure is independent of depth then it cannot achieve the optimal $\varepsilon^{2/3}L^{1/3}$ scaling law.

These insights are consistent with the present understanding of the intermediate state.

Our focus on energy minimization has the strength of permitting rigorous analysis. It has, however, corresponding weaknesses. We do not identify the actual geometry of any metastable state. And we do not address the processes by which domain patterns nucleate or change.

The paper is organized as follows: Section 2 provides physical and mathematical background. Section 3 gives a mathematically precise formulation of the underlying variational problem, and a more complete summary of our main results. Section 4 discusses the upper bounds associated with several constructions. Section 5 shows that our constructions are more or less optimal, given their topology. The analysis of Sections 4 and 5 shows that, except in the regime of Section 4.5, the energy of a domain pattern is mainly determined by its local length scale. Section 6 highlights this conclusion—and clarifies the constructions of Section 4—by discussing one-dimensional variational problems for optimizing the local length scale. Section 7 presents our ansatz-free lower bounds. Finally Section 8 concludes with a brief discussion.

The ansatz-free lower bounds in Section 7 scale optimally for intermediate values of $b_a$. However, they do not get the optimal prefactor in $b_a$ near 0 or 1. Improved bounds, with optimal scalings in $b_a$ or $1 - b_a$ (for $b_a$ near 0 and 1 respectively) will be presented in a forthcoming paper with S. Conti [12].

## 2. Background

This section reviews our present understanding of the intermediate state. This discussion is, we think, useful for appreciating the significance of our results. However it is not strictly speaking necessary for understanding the mathematics; the impatient reader can skip directly to Section 3.

### *2.1. The Intermediate State as a Nonconvex Variational Problem*

Superconductivity can be modeled in a number of different ways. We take a variational, sharp-interface viewpoint, following a long tradition begun by Landau [33]; for more general treatments see e.g. Huebener [23] or Tinkham [43]. The basic variable is the magnetic field $\mathbf{B}$, which is divergence-free. The superconducting material occupies a region $\Omega \subset R^3$. The material is characterized by a critical field $b_c$, above which it loses its superconducting properties. In most of this paper we choose units so that $b_c = 1$. For the following discussion, however, we avoid this convention for the sake of clarity.

We wish to model the effect of an applied field $\mathbf{b_a} = (b_a, 0, 0)$, assumed constant, by solving an appropriate variational problem. In any subset of $\Omega$ that remains supercon-

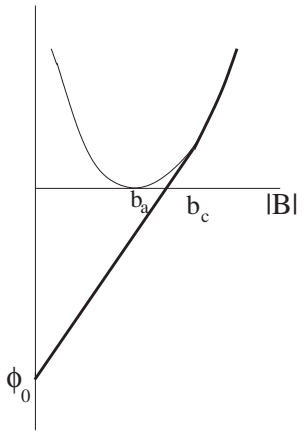


**Fig. 1.** The free energy $\phi$ and its convexification (bold).

ducting we have $\mathbf{B} = 0$, as a consequence of the Meissner effect. For reasons that will become clear below, the free energy density of this superconducting state takes the value

$$\phi_0 = b_a^2 - b_c^2 < 0 \tag{2.1}$$

when the magnitude of the applied field is $b_a$. We expect some regions of $\Omega$ to become nonsuperconducting (normal). In such regions we have $\mathbf{B} \neq 0$, and the free energy density is $\phi(\mathbf{B}) = |\mathbf{B} - \mathbf{b_a}|^2$. Outside $\Omega$ the free energy is likewise $|\mathbf{B} - \mathbf{b_a}|^2$. Ignoring for the moment the interfacial energy of the superconductor-normal interfaces, we arrive at the variational problem

$$\min_{\operatorname{div}\mathbf{B}=0} \int_\Omega \phi(\mathbf{B}) \; + \int_{\Omega^c} |\mathbf{B} - \mathbf{b_a}|^2, \tag{2.2}$$

with

$$\phi(\mathbf{B}) = \begin{cases} \phi_0 & \text{if } \mathbf{B} = 0, \\ |\mathbf{B} - \mathbf{b_a}|^2 & \text{if } \mathbf{B} \neq 0. \end{cases}$$

The free energy $\phi$ is nonconvex (see Figure 1). Therefore it can prefer mixtures over pure states; more precisely, energy minimization sometimes requires a microscopic mixture of superconducting and normal domains. This is the *intermediate state*. Its effective (locally averaged) energy is described by the convexification of $\phi$, evaluated at the locally averaged magnetic field (commonly called the magnetic induction). This was known already to Landau in 1937, and is discussed in the monographs cited above. From the mathematical viewpoint, (2.2) can be viewed as a nonconvex variational problem in need of relaxation; see e.g. [14], [32].

The convexification of $\phi$ is easy to calculate. For the rest of Section 2.1, we denote by $\overline{\mathbf{B}}$ the locally averaged field. Since $|\mathbf{B}-\mathbf{b_a}|^2$ is convex, we need only consider oscillations of $\mathbf{B}$ taking two values: $\overline{\mathbf{B}}/\lambda$ on volume fraction $\lambda$, and 0 on volume fraction $1 - \lambda$:

$$\phi_{\text{con}}(\overline{\mathbf{B}}) = \min_{0\le\lambda\le 1} \left\{ \lambda \left| \frac{\overline{\mathbf{B}}}{\lambda} - \mathbf{b_a} \right|^2 + (1-\lambda)\phi_0 \right\} . \tag{2.3}$$

A brief calculation shows that the optimal choice of $\lambda$ occurs when

$$\frac{|\overline{\mathbf{B}}|}{\lambda} = (b_a^2 - \phi_0)^{1/2} = b_c \ .$$

Thus, in the mixture, the magnitude of the magnetic field oscillates between 0 and the critical value $b_c$; our choice of $\phi_0$ in (2.1) was specifically designed to reach this result. Completing the convexification calculation: For a given (locally averaged) field $\overline{\mathbf{B}}$, the volume fraction of normal material is $\lambda = |\overline{\mathbf{B}}|/b_c$ if this is less than one and $\lambda = 1$ otherwise, and the value of the relaxed energy (2.3) is easily seen to be

$$\phi_{\text{con}}(\overline{\mathbf{B}}) = \phi_0 - 2\langle \overline{\mathbf{B}}, \mathbf{b_a} \rangle + \begin{cases} 2b_c|\overline{\mathbf{B}}| & \text{if } |\overline{\mathbf{B}}| \le b_c, \\ |\overline{\mathbf{B}}|^2 + b_c^2 & \text{if } |\overline{\mathbf{B}}| \ge b_c \ . \end{cases} \tag{2.4}$$

The thermodynamic theory of the intermediate state determines the locally averaged magnetic field $\overline{\mathbf{B}}$ by solving the relaxed variational problem:

$$\min_{\text{div}\,\overline{\mathbf{B}}=0} \int_\Omega \phi_{\text{con}}(\overline{\mathbf{B}}) \ + \int_{\Omega^c} |\overline{\mathbf{B}} - \mathbf{b_a}|^2.$$

For most domains $\Omega$ the solution is nonconstant and must be sought numerically. However the situation simplifies considerably when $\Omega$ is a plate, because the optimal $\overline{\mathbf{B}}$ is then constant throughout $\Omega$ and equal to $\mathbf{b_a}$ outside $\Omega$. The simplest case—the focus of this paper—is that of a plate oriented transverse to the applied field: Then the optimal $\overline{\mathbf{B}}$ is identically equal to $\mathbf{b_a}$. Indeed, the relaxed variational problem is convex, and this choice of $\overline{\mathbf{B}}$ is obviously admissible, with first variation equal to 0. (We have skipped over a technical point: If the plate has infinite extent, then the energy is formally infinite. We shall resolve this difficulty by imposing periodic boundary conditions in the longitudinal directions.)

Thus, for a flat plate in a transverse applied field, the thermodynamic (relaxed) theory predicts an intermediate state when the applied field satisfies $0 < b_a < b_c$. The volume fraction of normal material is $b_a/b_c$, and that of the superconducting material $1 - b_a/b_c$.

### *2.2. The Intermediate State as a Pattern-Formation Problem*

The thermodynamic theory just presented gives, as its main prediction, the local volume fraction of normal material. This prediction compares well with experiments—for example, with measurements of the overall magnetization.

However experiments show more than just volume fractions: They also reveal the *spatial structure* of the normal and superconducting regions. The review article by Livingston and DeSorbo [37] gives a good summary of the phenomenology, with many photographs. The structures seen are quite complex, with considerable hysteresis—details are rarely reproducible, and even the qualitative, topological characteristics can be history-dependent. Obviously the system has many metastable states and a very complicated bifurcation diagram.

This sort of situation is common in condensed matter physics. Energy minimization can still be a useful tool, though the system clearly does not achieve a globally energy-minimizing state. A common approach is to minimize energy numerically, or analytically

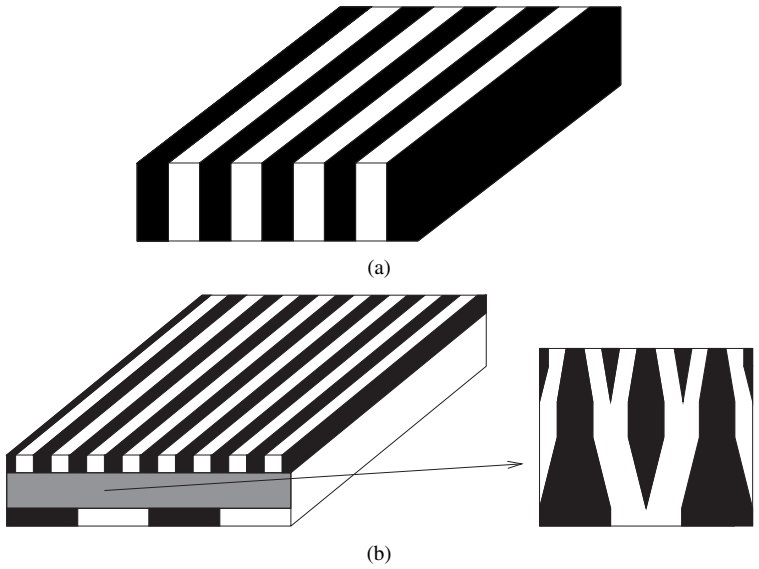

**Fig. 2.** Schematic examples of (a) a plate with a layered, unbranched domain structure, and (b) a plate with a layered, branched domain structure. The black regions superconduct, while the white regions are normal.

within a suitable ansatz. Then the "local minimum" is determined by the initial guess or the choice of ansatz.

The viewpoint of the present paper is different and more global. We aim to evaluate, at least approximately, the minimum value of the energy, and to identify common features of all near-minimum-energy states. If, as seems plausible, the accessible metastable states have relatively low energies, then the features we identify will apply to them as well as to the global energy-minimizing state.

What energy to minimize? Certainly not (2.2). That functional, being nonconvex, does not achieve its minimum. As Landau already understood, it must be augmented by including the surface energy of the normal-superconductor interfaces:

$$\min_{\operatorname{div}\mathbf{B}=0} \int_\Omega \phi(\mathbf{B}) \; + \int_{\Omega^c} |\mathbf{B}-\mathbf{b_a}|^2 \; + \varepsilon b_c^2 \, [\text{Interfacial Area}]\,, \tag{2.5}$$

where "interfacial area" refers to the total area of all normal-superconductor interfaces within $\Omega$, and $\varepsilon > 0$ is the surface tension (with dimensions of length). This formulation is too informal for mathematical analysis—we shall be more precise below—but it is sufficient for the present heuristic discussion. We emphasize that the inclusion of surface energy does much more than simply restore existence of a minimum. Physically, the surface energy—though small in magnitude—is dominant at small length scales where the details of pattern formation occur. Mathematically it is a singular perturbation, which regularizes the functional and selects the correct microstructures.

What should we hope to learn from energy minimization? In view of the complexity and hysteresis observed in experiments, it is not reasonable to seek the exact form of the energy-minimizing domain pattern. Rather, the appropriate goals are to understand

(a) The *microstructural length scale*: How does it depend on $\varepsilon$? Is it more or less uniform, or does it coarsen away from the faces of the plate?
(b) The *cross-sectional topology*: For example, is a layered geometry significantly better or worse than one with threads of normal material in a matrix of superconductor, or tunnels of superconductor in a matrix of normal?
(c) The *cross-sectional complexity*: Is there an energetic incentive for complexity? In other words, do the relatively disordered, labyrinthine structures observed experimentally achieve significantly lower energies than more ordered structures such as laminar geometries?

The literature includes many attempts to answer these questions by minimizing (2.5) within a suitable ansatz. We restrict our attention to work concerning a plate in a transverse applied field. Landau's initial 1937 treatment [33] considered a 2D (layered) pattern of normal and superconducting domains, flared a bit at the faces of the plate but otherwise uniform (the flaring is energetically unimportant, see [15], so this construction is basically the one shown in Figure 2a). In 1943, Landau realized that a branched-layered microstructure does better if the surface energy is small enough [34] (see Figure 2b). Landau also noted that the branched construction does not require a layered geometry; something similar can be done using normal threads in a matrix of superconductor, and this construction is preferred when the volume fraction of normal material is small. Andrews pursued this theme in 1948 [1], giving a careful treatment of the branched-thread construction (roughly equivalent to our Section 4.3). Experiments by Balashova and Sharvin in 1957 revealed that domain patterns often have two distinct length scales: a longer one associated with labyrinthine structure, and a shorter one associated with corrugations superimposed on that structure [2]. In 1958, Faber explained that corrugation provides an alternative means of changing the local length scale—different from but energetically equivalent to branching—and showed that when $\varepsilon$ is sufficiently small a layered configuration is unstable to corrugation [18]. This work strongly suggests certain answers to our first two questions:

(a′) When $\varepsilon$ is small enough compared to the thickness of the plate, the microstructural length scale should vary with depth. In other words, it should be larger in the middle of the plate than at the faces.
(b′) At intermediate volume fractions there is little energetic difference between different constructions with similar length scales. At the extreme volume fractions, however, thin threads or tunnels of one phase in a matrix of the other are preferred over laminar patterns.

Our results provide fresh support for these conclusions. With regard to (a′) they are quite conclusive: We show that the length scale must vary with depth, because if it doesn't (more precisely, if the entire domain pattern is independent of depth), then the minimum energy scales as $E_1 \sim \varepsilon^{1/2} L^{1/2} \gg \varepsilon^{2/3} L^{1/3}$.

With regard to (b′), our results are most novel in the small-$b_a$ regime. It was already recognized by Landau and Andrews that a uniform distribution of branched flux tubes do better than a laminar geometry; this is basically an isoperimetric effect—circular cross-sections have less surface energy. But we show, for the first time, that if $b_a \ll (\varepsilon/L)^{2/7}$, then it is not optimal for the flux tubes to be uniformly distributed;

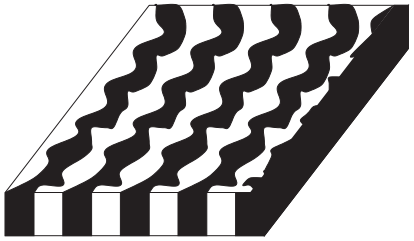

**Fig. 3.** Rough sketch of a plate with a complex but unbranched domain structure.

one gets a better scaling law by arranging them in clusters. This is basically a fringe-field effect: clustering reduces the exterior magnetic energy. We deduce that for very small applied fields the cross-sectional geometry should have two distinct length scales: the distance between tubes within a cluster, and the distance between clusters themselves.

Question (c) is different: There is no ansatz for "cross-sectional complexity," so methods like those of Landau and Andrew are not relevant. There are of course different types of complexity. Small-scale corrugations near the faces represent one type; they change the local length scale, as noted by Faber, consistent with point (a′). Large-scale labyrinthine structures represent another type of complexity. The numerical work of Dorsey, Goldstein, and Jackson [15], [19] suggests the answer here:

(c′) The labyrinthine cross-sectional complexity arises not from a significant energetic mandate, but rather from degeneracy and hysteresis.

The model used in [15], [19] assumes that the domain structure is uniform throughout the plate. In view of (a′), this is appropriate only when $\varepsilon$ is large enough relative to the thickness of the plate, not the regime of focus here. But we agree with the conclusion (c′). Our geometry-independent results provide fresh, very different support for this conclusion, by showing that no pattern—no matter how complex or labyrinthine—can achieve a better scaling law than highly ordered constructions like those considered by Landau and Andrews.

Figures 2 and 3 serve to illustrate points (a′) and (c′). They give schematic examples of domain patterns that are (i) layered and unbranched, (ii) layered and branched, (iii) complex and unbranched. Our ansatz-independent lower bounds show there is a substantial energetic incentive for branching, but little incentive for unbranched complexity. Indeed, when $\varepsilon$ is small enough, the scaling law associated with a branched domain structure (Figure 2b) is better than the one associated with an unbranched structure (Figure 3) (Landau already knew this). Experimentally one often sees patterns combining features of Figure 2b and Figure 3: labyrinthine cross-sectional complexity, with superimposed corrugations to reduce the length scale near the faces of the plate (see e.g. [2], [18]). It is natural to ask whether such patterns may form because they achieve a better scaling law. The answer is no: They cannot do better than the optimal $\varepsilon^{2/3}L^{1/3}$ law, which is also achieved by the highly ordered, branched structure in Figure 2b. This is the impact of our ansatz-independent lower bound.

Point (c′) makes reference to degeneracy and hysteresis. The problem is degenerate in the sense that there are many different domain structures with approximately the same energy. Indeed, we show in Sections 5 and 6 that the main requirement for achieving the optimal scaling law is getting the local length scale right. As a result of this degeneracy, nucleation and hysteresis are very important. For example, under a small applied field, energy minimization prefers a structure of thin normal threads in a matrix of superconductor (see (b′)). As the applied field increases, the normal-thread/superconducting-matrix topology is maintained, not because energy minimization favors it at larger volume fractions, but rather because the energy is more or less indifferent.

We digress to highlight an open problem. Dzyaloshinksii [16] and Sharvin [42] observed in the late 1950s that the situation is very different when the applied field is oblique rather than transverse to the plate. The nonzero tangential component breaks the degeneracy and eliminates the complexity, quite reliably inducing a layered domain pattern. We suppose the layered state must be strongly preferred energetically in the presence of an oblique applied field. However we do not know a theoretical explanation why this is so.

Now an awkward but important point. We have emphasized that energy minimization requires the local length scale to vary with depth if the surface tension $\varepsilon$ and the plate thickness $L$ satisfy $\varepsilon/L \ll 1$. Yet in many experiments the local length scale seems roughly uniform. This puzzle was explained by Lifshitz and Sharvin in 1951 [36]. Briefly: the energy achievable using a variable length scale is about $C_v \varepsilon^{2/3} L^{1/3}$, while that achievable using a uniform length scale is about $C_u \varepsilon^{1/2} L^{1/2}$. The constants $C_u$ and $C_v$ depend somewhat on the choice of ansatz, but for reasonable choices they are of the same order of magnitude, with $C_v > C_u$. For typical materials and experiments $\varepsilon$ is of order $10^{-4}$cm, while $L$ is about 1cm, so the variable length-scale energy is better if $C_v/C_u < (\varepsilon/L)^{-1/6} \approx 4.6$. This is plausibly true—but perilously close to the margin. Examination of the constructions shows that for such a ratio of $\varepsilon/L$, the number of generations of refinement would be at most one or two. Perhaps corrugation is seen more often than branching because small corrugations achieve something like a fractional generation of refinement.

### *2.3. Remarks on the Sharp-Interface Model*

Our sharp-interface variational model is precisely the one considered by Landau [33], [34] and Andrews [1], among others. It can be derived, at least formally, from the more fundamental Ginzburg-Landau model. The correspondence is discussed in almost every exposition of the Ginzburg-Landau theory. Systematic treatments based on asymptotic analysis can be found in [6], [7], [8], [15], and a rigorous convergence result in a 1D (radial) setting is given in [5].

The main point is this: The Ginzburg-Landau theory predicts a *correlation length* $\xi$ and a *penetration depth* $\lambda$. The correlation length gives the minimum scale on which the superconducting order parameter can vary; the penetration depth gives the distance the magnetic field penetrates into a superconducting region. The surface tension $\varepsilon$ of a normal-superconducting interface has the form $\xi f(\kappa)$, where $\kappa =: \lambda/\xi$ is the Ginzburg-Landau parameter and $f(\kappa) > 0$ for $\kappa < 1/\sqrt{2}$. The distinguishing characteristic of a type-I superconductor is that the associated value of $\kappa$ is less than $1/\sqrt{2}$.

In practice, a sharp-interface model is appropriate if the correlation length is small compared to the length scale of the domain structure. For typical type-I superconductors the penetration depth is $\lambda \sim 10^{-6}$cm and the correlation length is $\xi \sim 10^{-4}$cm, while for a 1cm-thick plate in a transverse field, the length scale of the domain structure is about $10^{-2}$cm. So the sharp-interface framework should be adequate.

### *2.4. The Link to Micromagnetics*

Many authors have noted the existence of an analogy between the domain structures in a uniaxial ferromagnet and those seen in the intermediate state of a type-I superconductor. Briefly: The two problems have similar preferences, but the type-I superconductor is more constrained. To explain in greater detail, we focus on the case of a uniaxial ferromagnetic plate, with the easy axis and the applied magnetic field both oriented in the transverse ($x_1$) direction. Then the magnetization $\mathbf{m}$ prefers two special values, $(\pm 1, 0, 0)$, and it prefers to be divergence-free; deviations are penalized by the anisotropy and magnetostatic terms of the micromagnetic variational principle. For a plate-shaped type-I superconductor in a transverse magnetic field, by contrast, the magnetic field $\mathbf{B}$ prefers to take the value $(b_c, 0, 0)$ in the normal phase, but it is constrained to be 0 in the superconducting phase, and it is constrained to be divergence-free.

How can this analogy be used? One alternative is to argue that there is no physically significant difference between the constrained and penalized versions; this is, roughly speaking, the starting point of [15], [19]. But there is also a second, more variational alternative: Every test field for the constrained problem determines a related test field for the unconstrained one. The value of this viewpoint is demonstrated in Section 7, where we apply it to deduce our ansatz-free lower bounds from the results of [11].

## 3. The Variational Problem ($\mathcal{P}$)

Section 3.1 gives a precise formulation of the singularly perturbed variational problem (2.5). Then Section 3.2 gives a variational characterization ($\mathcal{P}$) for the correction due to positive surface energy—the term $E_1$ of (1.1). Problem ($\mathcal{P}$) is the mathematical focus of the rest of this article. Section 3.3 explains our use of (standard but perhaps not universal) symbols like $\lesssim$, $\gtrsim$, and $\cong$. Finally, Section 3.4 summarizes our main mathematical results.

### *3.1. A Precise Formulation with Surface Energy*

Nondimensionalizing the magnetic fields, we henceforth take the critical field to be $b_c = 1$. The applied field is then $\mathbf{b_a} = (b_a, 0, 0)$ with $0 < b_a < 1$. The region occupied by the superconductor is a plate of thickness $L$, orthogonal to this field.

To avoid edge effects, and to facilitate spatial averaging, we restrict our attention to patterns that are spatially periodic in the plane of the plate. The choice of period is unimportant, provided it is large compared to the length scale of the microstructure. To

simplify notation, we set it to 1, i.e. we take $Q = [0, 1]^2$ as the two-dimensional period cell. A representative volume of the plate is thus

$$\Omega = (0, L) \times Q,$$

and a representative volume of its complement is correspondingly

$$\Omega^c = [(-\infty, 0] \cup [L, \infty)] \times Q.$$

Our variational problem has two unknowns: the magnetic field and the domain pattern. We represent the latter by a function $\chi$ defined on the plate and periodic in $y$ and $z$, such that

$$\chi = \begin{cases} 1 & \text{in the superconducting regions,} \\ 0 & \text{in the normal regions.} \end{cases}$$

Notice that the interfacial area is simply the total variation of $\chi$:

$$\text{interfacial area} = \int_\Omega |\nabla \chi|.$$

The constraint that $B$ vanish in the superconducting regions is easy to express: It says $B\chi = 0$ on $\Omega$. Our precise formulation of (2.5) is thus

$$\begin{array}{cc} \min & E(\mathbf{B}, \chi), \\ \operatorname{div} \mathbf{B} = 0, & \\ \mathbf{B}\chi = 0 \text{ in } \Omega, & \end{array} \tag{3.1}$$

with

$$E(\mathbf{B}, \chi) = \int_\Omega \left( |\mathbf{B} - \mathbf{b_a}|^2 - \chi \right) dx\, dy\, dz + \varepsilon \int_\Omega |\nabla \chi| + \int_{\Omega^c} |\mathbf{B} - \mathbf{b_a}|^2 \, dx\, dy\, dz. \tag{3.2}$$

Here $\mathbf{B}$ ranges over all $L^2_{\text{loc}}$ vector fields, periodic in $y$ and $z$, which satisfy $\operatorname{div} \mathbf{B} = 0$ in the sense of distributions; $\chi$ ranges over all characteristic functions, periodic in $y$ and $z$, with finite total variation; and $\mathbf{B}\chi = 0$ in $\Omega$ means $B = 0$ almost everywhere on the set where $\chi = 1$.

We expect the inclusion of surface energy to assure the existence of a minimizer. Our problem (3.1) has this property for any $\varepsilon > 0$. The proof is a standard application of the direct method of the calculus of variations. The only novelty is the constraint $\mathbf{B}\chi = 0$; we must check that it holds for the weak limits $\mathbf{B}_*$ and $\chi_*$ of a minimizing sequence $\mathbf{B}_j$, $\chi_j$. This is easy: Such a sequence has $\int_\Omega |\nabla \chi_j|$ uniformly bounded, so the $\chi_j \to \chi_*$ strongly in $L^1$. Therefore the product $\mathbf{B}_j \chi_j$ converges weakly to the product of the limits $\mathbf{B}_* \chi_*$. Since $\mathbf{B}_j \chi_j = 0$ for all $j$, we conclude that $\mathbf{B}_* \chi_* = 0$ as well.

We remark that (3.1) is not the only reasonable interpretation of (2.5). A different alternative would have been to define the superconducting region as the set where $\mathbf{B} = 0$. This amounts to slaving slave $\chi$ to $\mathbf{B}$ by

$$\chi = \begin{cases} 1 & \text{where } \mathbf{B} = 0, \\ 0 & \text{where } \mathbf{B} \neq 0. \end{cases} \tag{3.3}$$

We dislike this alternative because the resulting energy is not lower semicontinuous—the perimeter of the set where $\mathbf{B} = 0$ can change drastically under weak convergence. Therefore the existence of a minimizer cannot be proved by the direct method of the calculus of variations. Our interpretation is less than or equal to the slaved one, since the choice (3.3) is admissible for (3.1). Therefore the geometry-independent lower bounds we prove for (3.1) hold a fortiori for the slaved interpretation as well.

### *3.2. A Variational Problem* $(\mathcal{P})$ *for the Principal-Order Correction*

We know, from general considerations, that the leading-order term $E_0$ in our (conjectured) expansion of the energy is the minimum of the convexified problem. For a plate in a transverse field it is achieved at $\mathbf{B} = \mathbf{b_a}$, so we deduce from (2.4) that

$$E_0 = \int_\Omega \phi_{\text{con}}(\mathbf{b_a}) = -(b_a - 1)^2 L. \tag{3.4}$$

But our real interest is in the principal-order correction $E_1$ associated with positive surface energy. We claim that this correction is itself given by a variational problem, namely

$$(\mathcal{P}) \qquad \min_{\substack{\operatorname{div}\mathbf{B} = 0 \\ \mathbf{B}\chi = 0 \text{ in } \Omega}} \int_\Omega \left[B_2^2 + B_3^2 + (1-\chi)(B_1 - 1)^2\right] dx\, dy\, dz + \varepsilon \int_\Omega |\nabla \chi| + \int_{\Omega^c} |\mathbf{B} - \mathbf{b_a}|^2\, dx\, dy\, dz.$$

In the course of proving this, we shall also give a self-contained proof of (3.4). The argument makes use of the following simple lemma:

**Lemma 3.1.** *For any divergence-free* $\mathbf{B}$*, periodic in* $y$ *and* $z$*, if* $\int_{\Omega^c} |\mathbf{B} - \mathbf{b_a}|^2\, dx\, dy\, dz < \infty$*, then for every* $x \in (0, L)$ *we have*

$$\int_Q B_1(x, y, z)\, dy\, dz = b_a. \tag{3.5}$$

*Proof.* The divergence-free property together with the periodicity hypothesis give

$$\frac{\partial}{\partial x} \int_Q B_1\, dy\, dz = -\int_Q \left(\frac{\partial B_2}{\partial y} + \frac{\partial B_3}{\partial z}\right) dy\, dz = 0.$$

So the left-hand side of (3.5) is independent of $x$ for all $x \in \mathbf{R}$. Its value must be $b_a$ since otherwise $\int_{\Omega^c} |\mathbf{B} - \mathbf{b_a}|^2\, dx\, dy\, dz$ would be infinite. □

We turn now to the justification of $(\mathcal{P})$. By Lemma 3.1 we have

$$\int_\Omega \left[b_a^2 - 1 + 2(1 - b_a) B_1\right] dx\, dy\, dz = -(b_a - 1)^2 L.$$

Therefore our energy (3.2) can be expressed as

$$E(\mathbf{B}, \chi) = -(b_a - 1)^2 L + \int_\Omega |\mathbf{B} - \mathbf{b_a}|^2 - \chi - [b_a^2 - 1 + 2(1 - b_a)B_1]\, dx\, dy\, dz + \varepsilon \int_\Omega |\nabla \chi| + \int_{\Omega^c} |\mathbf{B} - \mathbf{b_a}|^2\, dx\, dy\, dz.$$

Since $\mathbf{B}\chi = 0$ on $\Omega$, the integrand of the second line is

$$|\mathbf{B} - \mathbf{b_a}|^2 - \chi - [b_a^2 - 1 + 2(1 - b_a)B_1] = B_2^2 + B_3^2 + (1 - \chi)(B_1 - 1)^2.$$

Thus for any admissible $\chi$ and $\mathbf{B}$, we have

$$E(\mathbf{B}, \chi) = -(b_a - 1)^2 L + \int_\Omega \left[B_2^2 + B_3^2 + (1 - \chi)(B_1 - 1)^2\right] dx\, dy\, dz + \varepsilon \int_\Omega |\nabla \chi| + \int_{\Omega^c} |\mathbf{B} - \mathbf{b_a}|^2\, dx\, dy\, dz.$$

To complete the argument we must show that the minimum value of $(\mathcal{P})$ tends to 0 as $\varepsilon \to 0$. The following lemma proves this, and even gives a rate. The proof is by now standard, but we give it anyway for the reader's convenience.

**Lemma 3.2.** *As $\varepsilon \to 0$, the minimum value of $(\mathcal{P})$ is at most $C\varepsilon^{1/2}L^{1/2}$, where $C > 0$ depends on $b_a$ but not on $\varepsilon$ or $L$.*

*Proof.* Consider an arrangement of superconducting and normal layers oriented perpendicular to the $z$ axis, with volume fraction $1 - b_a$ of superconductor. To express this mathematically, define a function $\zeta(z)$ for $0 \le z \le 1$ by

$$\zeta = \begin{cases} 1 & \text{if } 0 \le z \le \frac{1-b_a}{2} \text{ or } \frac{1+b_a}{2} \le z \le 1, \\ 0 & \text{if } \frac{1-b_a}{2} < z < \frac{1+b_a}{2}, \end{cases}$$

then extend $\zeta$ to all $z \in \mathbf{R}$ by periodicity. The layered microstructure we wish to consider is associated with $\chi = \chi_m(x, y, z) = \zeta(x, y, mz)$ where $m$ is a large integer. As a test function for the magnetic field, we define $\mathbf{B}_m$ separately inside and outside of $\Omega$. Inside, we set $\mathbf{B}_m = (\theta_m, 0, 0)$ where

$$\theta_m(x, y, z) = \begin{cases} 0 & \text{if } \chi_m(x, y, z) = 1, \\ 1 & \text{if } \chi_m(x, y, z) = 0. \end{cases}$$

Outside, we set $\mathbf{B}_m = \nabla u + \mathbf{b_a}$, where $u$ is the $(y, z)$-periodic solution on $\Omega^c$ of the boundary value problem

$$\Delta u = 0, \qquad u_x(L, y, z) = \theta_m(L, y, z) - b_a, \qquad u_x(0, y, z) = \theta_m(0, y, z) - b_a.$$

Notice that $\operatorname{div} \mathbf{B}_m = 0$ since the normal component of $\mathbf{B}_m$ is continuous at $x = \pm L$. The associated principal-order correction to the energy is

$$\begin{aligned} E_1(\chi_m, \mathbf{B}_m) &= \varepsilon \int_\Omega |\nabla \chi_m| + \int_{\Omega^c} |\nabla u|^2 \\ &\lesssim \varepsilon m L + \|\theta_m(L, \cdot, \cdot) - b_a\|^2_{H^{-\frac{1}{2}}(Q)} \\ &\lesssim \varepsilon m L + C(b_a)\frac{1}{m} \end{aligned} \tag{3.6}$$

(see the appendix for a discussion of the space $H^{-\frac{1}{2}}$ and its norm). The result follows easily, by optimizing the microstructural length scale $1/m$. □

*Remark.* We are, in general, interested in the dependence of our prefactors on $b_a$. The proof of Lemma 3.2 actually shows that

$$\min(\mathcal{P}) \le C\, b_a\, |\log b_a|^{1/2}\, (1-b_a)\, |\log(1-b_a)|^{1/2}\, \varepsilon^{1/2}\, L^{1/2},$$

with $C$ independent of $b_a$. It suffices to use the full force of Proposition A.2 from the appendix, which specifies the dependence of $\|\theta_m(L, y, z) - b_a\|^2_{H^{-\frac{1}{2}}(Q)}$ on $b_a$.

### *3.3. Some Notation*

We fix a notation for *inequalities up to some fundamental unspecified constant*. For functions $f$ and $g$ of certain parameters, let us agree that:

(1) $f \lesssim g$ (respectively $f \gtrsim g$) means there exists some fundamental constant $C$ (independent of all parameters) such that $f \le Cg$ (respectively, $f \ge Cg$).
(2) $f \sim g$ means $f \lesssim g$ and $f \gtrsim g$; in other words, there exist fundamental constants $c$ and $C$ such that $cg \le f \le Cg$.
(3) $f \cong g$ means there exists a fundamental constant $C$ such that $f = Cg$.

If a prefactor depends on $b_a$, then we shall make this dependence explicit, as in (3.6) above. We sometimes write $C$, $c$, etc., for a generic fundamental constant that may vary from line to line.

### *3.4. Summary of Our Main Results*

We have shown that problem $(\mathcal{P})$ captures precisely the energetic correction due to positive surface tension. This variational problem will be the focus of our attention henceforth. We aim (i) to identify the optimal scaling law for its minimum value, and (ii) to understand what features a domain structure must possess to achieve this scaling law.

Upper bounds for the scaling law are obtained by considering specific constructions. The proof of Lemma 3.2 gives one such bound, namely $\min \mathcal{P} \le C(b_a)\varepsilon^{1/2}L^{1/2}$. But as Landau observed in 1943, a branched construction does better if $\varepsilon/L \ll 1$; and as Andrews observed in 1948, a branched-flux-tube microstructure does better than layers if $b_a$ is close to 0. We review these constructions in Sections 4.1 to 4.3. We also show the existence of another, previously unrecognized alternative in Section 4.5. Its flux tubes branch but remain clustered—roughly speaking, it interpolates between Andrews's branched construction (where the flux tubes are uniformly distributed) and an unbranched structure (the ultimate extreme of clustering). Our new construction does better than the others for the smallest values of $b_a$. Taken together, these arguments show that for $b_a$ near 0,

$$\min \mathcal{P} \lesssim b_a \varepsilon^{4/7} L^{3/7}, \qquad \text{for } b_a \lesssim (\varepsilon/L)^{2/7}, \tag{3.7}$$

$$\min \mathcal{P} \lesssim b_a^{2/3} \varepsilon^{2/3} L^{1/3}, \qquad \text{for } (\varepsilon/L)^{2/7} \lesssim b_a. \tag{3.8}$$

For intermediate values of $b_a$, Landau's branched layered construction (Sections 4.1–4.2) and Andrews's branched flux tube construction (Section 4.3) give the same scaling law:

$$\min \mathcal{P} \lesssim \varepsilon^{2/3} L^{1/3}, \quad \text{for } b_a \text{ bounded away from 0 and 1.} \tag{3.9}$$

The situation near $b_a = 1$ is not symmetric to that near $b_a = 0$, because the superconducting and normal phases are physically quite different. The analogue of Andrews's construction for near-critical $b_a$ uses branched superconducting tunnels. It too seems to be new; we describe it in Section 4.4. This construction shows that for $b_a$ near 1,

$$\min \mathcal{P} \lesssim (1 - b_a)\,|\log(1 - b_a)|^{1/3} \varepsilon^{2/3} L^{1/3} \quad \text{if } \varepsilon/L \lesssim |\log(1 - b_a)|^{-2}. \tag{3.10}$$

If $b_a$ is large enough, there will be no superconducting region. That corresponds to $\chi = 0$, $\mathbf{B} = (b_a, 0, 0)$, achieving

$$\min \mathcal{P} \lesssim (1 - b_a)^2 L.$$

This scaling law does better than (3.10) when $(\varepsilon/L)^{2/3} \gg (1 - b_a)|\log(1 - b_a)|^{-1/3}$.

Most of these bounds are optimal, or nearly so, as we shall explain presently. To prove such a statement, one requires ansatz-independent lower bounds. For surface energy this is a familiar topic—the standard isoperimetric inequality amounts to an ansatz-independent lower bound on surface energy at given volume. We are, however, not aware of prior work on ansatz-independent lower bounds for magnetic energy.

The constructions in Section 4 provide a convenient starting point for addressing this issue. Each has a branched, periodic structure, and it is natural to ask whether the unit cell has been chosen more or less optimally. There are two distinct issues: Have we made a good choice of the interior geometry (expressed by $\chi$)? And have we done a good job of estimating the magnetic energy (associated with $\mathbf{B}$)? Section 5 addresses these issues. Its main result, Proposition 5.1, is a lower bound on the magnetic energy between a pair of given cross-sections.

Proposition 5.1 shows, as an immediate consequence, that the "branched" constructions of Sections 4.1 to 4.4 are more or less optimal. In particular, it provides matching lower bounds for (3.8) and (3.9), and a nearly matching lower bound for (3.10), for all microstructures of the type considered in Section 4. These are not exactly ansatz-independent bounds, since they assume a branched structure. Still, they show that the detailed structure of the flux tubes hardly matters; rather, what matters is the geometry and topology of a typical cross-section.

The main requirement for achieving the $\varepsilon^{2/3} L^{1/3}$ scaling law seems to be that the *local length scale* have the proper dependence on $x$. Section 6 emphasizes this feature of the problem by introducing a family of "toy problems" for the local length scale $h(x)$. These scalar variational problems permit us to concentrate on the essential physics—the topological type of the microstructure, and the choice of the local length scale. Since they are easy to analyze, the toy problems make it easy to understand the basic structure of the problem. In particular, the scaling law associated with each construction is immediately evident from the associated toy problem, by nondimensionalization. Our toy problems seem to be new as a technique for understanding the intermediate state; however, a similar idea was used long ago by Hubert to analyze the domain structure of a uniaxial

ferromagnet [21]. There is no toy problem for the construction of Section 4.5—involving clustered, branched flux tubes, and associated with (3.7)—because that microstructure has two length scales rather than one.

The analysis in Sections 5 and 6 tells us what can and cannot be achieved using a branched periodic construction. It does not however address the impact of cross-sectional complexity. Might such complexity serve to reduce the energy, as a substitute for branching? The answer is no. We show this in Section 7.2, by proving that for intermediate values of $b_a$, if the microstructure is independent of $x$, then it cannot do better than $\varepsilon^{1/2}L^{1/2}$, regardless of its cross-sectional geometry and complexity:

$$\text{value of } (\mathcal{P}) \gtrsim \varepsilon^{1/2}L^{1/2}$$
$$\text{for } x\text{-independent structure, and } b_a \text{ bounded away from 0 and 1.}$$

This bound is truly ansatz-independent, in the sense that it assumes *nothing* except $x$-independence. The $\varepsilon^{1/2}L^{1/2}$ scaling law is achieved by a layered microstructure. Thus at the level of the scaling law there is no energetic incentive for cross-sectional complexity.

What about complexity combined with branching? For example, Faber observed that the local length scale can be changed using corrugation rather than branching. Can such a construction (or another as-yet unimagined pattern) beat the highly regular ones considered in Section 4? The answer is no, at least at the level of the scaling law, for intermediate values of $b_a$. Indeed, we show in Section 7.2 that for any domain pattern, of any complexity and with any dependence on $x$,

$$\text{value of } (\mathcal{P}) \gtrsim \min\{b_a, (1-b_a)\}\varepsilon^{2/3}L^{2/3}$$
$$\text{provided } (\varepsilon/L)^{2/3} \lesssim b_a \text{ and } (\varepsilon/L)^{2/3} \lesssim (1-b_a). \tag{3.11}$$

This bound shows that the branched periodic constructions come within a constant of optimality so long as $b_a$ stays away from 0 and 1.

What must a domain pattern look like to achieve the $\varepsilon^{2/3}L^{1/3}$ scaling law? It is natural to conjecture that its local length scale, suitably defined, must resemble the solution of our "toy problem." What we can prove is a weaker statement: Its total surface energy, integrated in $x$, is similar to that of the branched periodic construction. This is discussed in Section 7.3.

The preceding discussion has focused on intermediate values of $b_a$—i.e. values far from 0 or 1. The situation is more complex for $b_a$ near 0 and near 1—reflected by our constructions achieving specific scalings involving $b_a$, cf. (3.7), (3.8), and (3.10). Ansatz-independent bounds matching these scalings will be presented in [12].

## 4. Guessing the Local Length Scale: New and Old Constructions

The proof of Lemma 3.2 showed that an unbranched, laminar domain structure achieves the scaling law $\varepsilon^{1/2}L^{1/2}$. This section presents several constructions of branched domain patterns that achieve the better scaling law $\varepsilon^{2/3}L^{1/3}$. One, discussed in Sections 4.1 and 4.2, is essentially due to Landau; it is two-dimensional (laminar). Another, discussed in Section 4.3, is essentially due to Andrews; it is three-dimensional, with thin tubes of the normal material in a matrix of superconductor. A third, discussed in Section

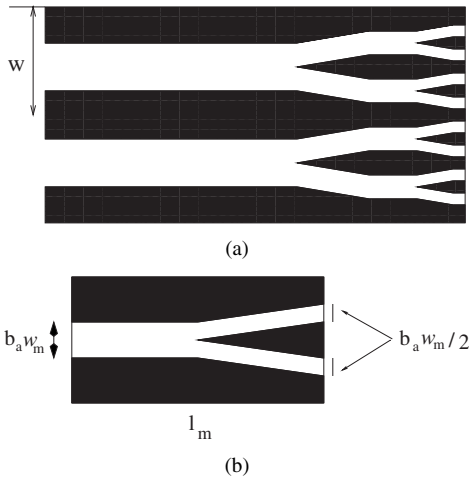


**Fig. 4.** (a) The 2D (laminar) construction with $N = 2$. The black regions are superconducting, and the applied field is $b_a < 1/2$. (b) The unit cell with length $l_m$ and height $w_m$.

4.4, is the large-applied-field analogue of Andrews's construction, with thin tubes of superconducting material in a matrix of normal. For intermediate values of $b_a$, all these constructions achieve roughly the same energy. For $b_a$ near 0 or 1, however, the 3D constructions do better. This is seen not in the $\varepsilon^{2/3}L^{1/3}$ scaling law, which remains the same, but rather in the dependence of the prefactor on $b_a$.

We also present a two-scale construction in Section 4.5. It does better than Andrews's construction when the applied field is sufficiently small. The geometry consists of flux tubes that branch but remain clustered.

The realizability of each construction requires some modest restrictions on the surface tension $\varepsilon$, the plate width $L$, and the applied field $b_a$—see (4.3), (4.4), (4.5), (4.8), and (4.19). In each case the condition has two parts. One requires that $\varepsilon^{1/3}L^{2/3}$ (which has the dimensions of length) be small enough compared to the periodicity of our unit cell $Q$. The other requires that the nondimensional ratio $\varepsilon/L$ be small enough. In most cases the smallness requirement on $\varepsilon/L$ is precisely the same as the condition that the construction do better than its unbranched analogue (this is easiest to see from the table in Section 6).

The constructions in Sections 4.1 to 4.4 all follow the same basic pattern. We sketch it now, concentrating for simplicity on the 2D version shown in Figure 4. In the center of the plate we have a periodic pattern with length scale $w$ consisting of a minority phase within the majority phase. As one approaches either face of the plate (the figure shows only the right half $x \geq L/2$), the minority domains (whether normal or superconducting) split in two. The process continues $N$ times; thus at the face of the plate the domain structure is similar to that in the center, but its length scale is much finer, $w/2^N$ rather than $w$. The details of the splitting are dictated by the choice of a basic cell structure, like that shown in Figure 4b. The cell structure is used at many different scales, so it

must be defined for all values of the cell height $w$ and cell length $l$—subject only to the *admissibility condition* that the slope of the superconductor-normal interface be at most of order 1. (For Figure 4, this requires $w \lesssim l$.)

To specify the construction, we must choose the height $w$ and length $l$ of the coarsest cells and the number of generations $N$ of refinement. We use the following *branching algorithm*, which abstracts Landau's analysis of the intermediate state and also related work by Privorotskii [39] on the domain structure of a uniaxial ferromagnet (see also [10]):

**Step 1:** Specify the geometry of the basic unit cell, for any admissible $w$ and $l$, and estimate its energy as a function of $w$ and $l$. Then optimize with respect to $l$ while holding $w$ fixed. This gives a formula for $l = l_{opt}(w)$, the optimal $l$ as a function of $w$.

**Step 2:** Setting $w_m = w/2^m$ and $l_m = l_{opt}(w_m)$, imagine for a moment using infinitely many generations of refinement. The energy can be evaluated by summing a geometric series. So can the total length $\sum_{m=1}^{\infty} l_m$. We choose $w$ so this total length is of order $L$: This gives a formula $w = w(\varepsilon, L, b_a)$ and lets us calculate the interior energy in terms of $\varepsilon$, $L$, and $b_a$.

**Step 3:** The infinitely branched construction anticipated in Step 2 is not permissible: it eventually violates the admissibility condition on the slope of the superconductor-normal interface. Therefore the branching process must be truncated after $N$ stages. We choose $N = N(\varepsilon, L, b_a)$ so that the exterior magnetic energy—estimated using the $H^{-1/2}$ norm as in the proof of Lemma 3.2—is comparable with the energy in the interior of the sample.

**Step 4:** One must check that this works. There are two conditions: First, Step 3 must give $N \gtrsim 1$; and second, the resulting $w_N$ and $l_N$ must be admissible. This leads to the two-part realizability condition for each construction.

The domain pattern obtained this way is dyadically branched, but it is not strictly speaking self-similar. Indeed, the aspect ratio of the period cell at the $m$th stage, $w_m/l_m$, is not independent of $m$, since $l_m$ is chosen to optimize the energy (Step 1) rather than chosen by geometric similarity.

Our branching algorithm is greedy, in the sense that we choose $l_m = l_{opt}(w_m)$ for each $w_m = w/2^m$. An apparently different alternative would be to let $l_m$ be arbitrary (subject to $\sum_m l_m = L$), then optimize the energy at the end. The greedy method is easier to present, since it eliminates $l_m$ as a degree of freedom as early as possible. But the other alternative gives the same result—indeed, the "toy problems" presented in Section 6 amount to an implementation of that idea.

The constructions presented here are very similar to those in our recent paper [10] on uniaxial ferromagnets. We shall therefore be fairly brief, referring the reader to that work for more detailed discussion.

A word is in order about Step 2. If the plate has thickness *exactly* $L$, why is it sufficient that $\sum_{m=1}^{\infty} l_m$ be *approximately* $L$? The answer is that the construction has a great deal of freedom. For example, we can change the choice of $l_m$ and therefore $\sum_{m=1}^{\infty} l_m$ by a constant factor without altering the energy scaling law.

### *4.1. The Branched, Layered Microstructure—Small Applied Field*

The initial steps of this 2D (laminar) construction are the same for large and small $b_a$. So for the moment we avoid placing any restriction on $b_a$.

The structure follows Figure 4, with the convention that the black regions are superconducting and the white regions normal. The basic unit cell is given in Figure 4b with $w_m = w/2^m$ and $l_m$ chosen appropriately. In drawing Figure 4, we have taken $b_a < 1/2$.

To present the construction mathematically, we shall construct a 2D vector field $\mathbf{B}(x, y)$ and a characteristic function $\chi(x, y)$. The associated 3D structure is naturally given by $\chi(x, y, z) = \chi(x, y)$ and $\mathbf{B}(x, y, z) = (\mathbf{B}(x, y), 0)$.

We must specify the test field for $\mathbf{B}$. In the superconducting regions (black in Figure 4) we must set $\mathbf{B} = 0$. In all horizontal normal regions we set $\mathbf{B} = (1, 0)$. In the $m$th cell (Figure 4b) we choose $\mathbf{B}$ to be piecewise constant, with

$$\mathbf{B} = \begin{cases} \left(1, \frac{(1-b_a)w}{2l}\right) & \text{in the white leg pointing northeast,} \\ \left(1, -\frac{(1-b_a)w}{2l}\right) & \text{in the white leg pointing southeast.} \end{cases} \tag{4.1}$$

The resulting $\mathbf{B}$ is divergence-free. In estimating its energy, we are only interested in how the result scales as $\varepsilon \to 0$ and $b_a \to 0$ or 1; therefore we shall ignore numerical constants of order 1. The admissibility condition on the slope of the superconductor-normal interface requires $w_m \lesssim l_m$ when $b_a$ is bounded away from 1, but only $(1 - b_a)w_m \lesssim l_m$ for $b_a$ near 1 (see Figure 5).

**Step 1:** For the energy $E_{cell}$ of the unit cell, we have

$$E_{cell} \lesssim \varepsilon\, l + \left((1 - b_a)\frac{w}{l}\right)^2 b_a\, w\, l \;=\; \varepsilon\, l + (1 - b_a)^2\, b_a\, \frac{w^3}{l}.$$

Optimization in $l$ gives

$$l_{opt}(w) \cong \frac{b_a^{1/2}\,(1 - b_a)w^{3/2}}{\varepsilon^{1/2}} \qquad \text{and} \qquad E_{cell} \lesssim \varepsilon^{1/2}\, b_a^{1/2}(1 - b_a)w^{3/2}.$$

**Step 2:** We set $w_m = w/2^m$ and $l_m = l_{opt}(w_m)$. Since there are $1/w$ cells that refine, we have

$$E_{inside} \lesssim \frac{1}{w} \sum_{m=1}^{\infty} 2^{m-1}\, \varepsilon^{1/2}\, b_a^{1/2}(1 - b_a)w^{3/2} \left(\frac{1}{2^m}\right)^{3/2} \lesssim \varepsilon^{1/2}\, b_a^{1/2}\,(1 - b_a)\, w^{1/2}.$$

Since $\{l_m\}$ is a geometric series, the condition $\sum l_m \cong L$ is equivalent to $l_{opt}(w) \cong L$. This gives

$$w \cong \frac{\varepsilon^{1/3}\, L^{2/3}}{b_a^{1/3}\,(1 - b_a)^{2/3}} \qquad \text{and} \qquad E_{inside} \lesssim b_a^{1/3}\,(1 - b_a)^{2/3}\,\varepsilon^{2/3}\, L^{1/3}. \tag{4.2}$$

From here the argument is slightly different for small versus large $b_a$. So we assume for the rest of this subsection that $b_a \leq 1/2$, and hence ignore factors involving $(1 - b_a)$. As we shall see, the realizability conditions for this regime are

$$\frac{\varepsilon^{1/3}\, L^{2/3}}{b_a^{1/3}} \lesssim 1 \qquad \text{and} \qquad \varepsilon/L \lesssim b_a^4\, |\log(b_a)|^3. \tag{4.3}$$

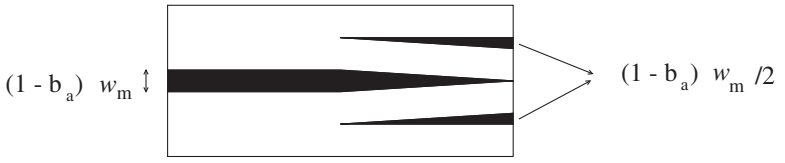


**Fig. 5.** The unit cell of the 2D branched construction at the $m$th stage, for $b_a \geq 1/2$. The vertical dimension is $w_m$ and the horizontal dimension is $l_m$.

The former says that $w \lesssim 1$ when $w$ is given by (4.2), so that the unit cell fits in our domain $\Omega$; the latter is needed in Step 4.

**Step 3:** We must choose an appropriate truncation. In view of Propositions A.1 and A.2 in the Appendix, the exterior magnetic energy will be less than or comparable to the interior energy if

$$E_{outside} \lesssim b_a^2 \,|\log b_a|\, w_N = \frac{b_a^2\,|\log(b_a)|\, w}{2^N} \cong b_a^{1/3}\,\varepsilon^{2/3}\,L^{1/3}, \;\text{ i.e. }\; w_N \cong \frac{\varepsilon^{2/3}\,L^{1/3}}{b_a^{5/3}\,|\log(b_a)|}.$$

**Step 4:** One readily checks that (4.3) implies

$$\frac{w_N}{l_N} \cong \frac{\varepsilon^{1/6}\,b_a^{1/3}\,|\log(b_a)|^{1/2}}{L^{1/6}} \lesssim 1 \qquad 2^N \cong \left(\frac{b_a^4\,|\log(b_a)|^3\,L}{\varepsilon}\right)^{1/3} \gtrsim 1.$$

Therefore the construction is realizable.

In summary, this 2D branched construction shows that

$$\min(\mathcal{P}) \lesssim b_a^{1/3}\,\varepsilon^{2/3}\,L^{1/3},$$

provided $b_a \leq 1/2$, if $\varepsilon$ and $L$ satisfy (4.3). For $b_a$ small, the branched thread construction of Section 4.3 will do better, achieving a prefactor of $b_a^{2/3}$ rather than $b_a^{1/3}$.

### *4.2. The Branched Layered Structure—Large Applied Field*

We turn now to the case $b_a \geq 1/2$ of Landau's 2D branched construction. As we shall see, the realizability conditions for this regime are

$$\frac{\varepsilon^{1/3}\,L^{2/3}}{(1-b_a)^{2/3}} \lesssim 1 \qquad \text{and} \qquad \varepsilon/L \lesssim (1-b_a)^2\,|\log(1-b_a)|^3. \tag{4.4}$$

The basic geometry was described in the previous section. All that change for $b_a \geq 1/2$ are the details of the truncation and the prefactor of the energy scaling law. The unit cell has the form shown in Figure 5. Notice that the slope of the superconductor-normal interface is of order $(1-b_a)w/l$; we require that this be at most of order 1 for the cell to be admissible.

From Steps 1 and 2 in Section 4.1 we have

$$w \cong \frac{\varepsilon^{1/3} L^{2/3}}{(1-b_a)^{2/3}} \qquad \text{and} \qquad E_{inside} \lesssim (1-b_a)^{2/3}\, \varepsilon^{2/3}\, L^{1/3}.$$

Notice that $w \lesssim 1$ by (4.4).

For Step 3, in view of Propositions A.1 and A.2 of the appendix, we take

$$w_N \cong \frac{\varepsilon^{2/3} L^{1/3}}{(1-b_a)^{4/3}\,|\log(1-b_a)|}.$$

This choice insures that the exterior energy is no larger than the interior energy.

For Step 4, we note using (4.4) that

$$\begin{aligned} \frac{(1-b_a)w_N}{l_N} &\cong (1-b_a)^{2/3}\,|\log(1-b_a)|^{1/2}\,(\varepsilon/L)^{1/6} \lesssim 1, \\ 2^N &\cong (1-b_a)^{2/3}\,|\log(1-b_a)|\,(L/\varepsilon)^{1/3} \gtrsim 1. \end{aligned}$$

Thus the 2D branched construction shows that

$$\min(\mathcal{P}) \lesssim (1-b_a)^{2/3}\,\varepsilon^{2/3}\,L^{1/3},$$

for $b_a \geq 1/2$, provided that $\varepsilon$ and $L$ satisfy (4.4). For $b_a$ large, the branched tunnel construction of Section 4.4 will do better, achieving a prefactor of $(1-b_a)\,|\log(1-b_a)|^{1/3}$ rather than $(1-b_a)^{2/3}$.

*Remark.* Comparison of Figures 4 and 5 reveals an important asymmetry between the normal and superconducting phases. The normal region consists of threads running the entire width of the plate, which carry magnetic flux from one side to the other. The superconducting region, on the other hand, consists mainly of islands that connect to just one face of the plate. This asymmetry is responsible for the different scaling of the prefactor in the two cases $b_a^{1/3}$ versus $(1-b_a)^{2/3}$. It is also reflected in our terminology for the 3D constructions—"normal threads" in a superconducting matrix, versus "superconducting tunnels" in a normal matrix. Finally, it is reflected in the slope of the normal-superconductor interface, which is of order $w_m/l_m$ for $b_a$ near 0, but $(1-b_a)\,w_m/l_m$ for $b_a$ near 1.

### *4.3. Thin Threads of Normal Material—Small Applied Field*

It was already noticed by Landau that when $b_a$ is sufficiently small, isoperimetric effects favor normal threads rather than layers. The first detailed discussion of such a structure was given by Andrews [1]. The following construction is similar to Andrews's.

We assume throughout this discussion that $b_a \leq 1/2$. We shall see that the realizability conditions for this construction are

$$\frac{\varepsilon^{1/3} L^{2/3}}{b_a^{1/6}} \lesssim 1 \qquad \text{and} \qquad \varepsilon/L \lesssim b_a^2. \tag{4.5}$$

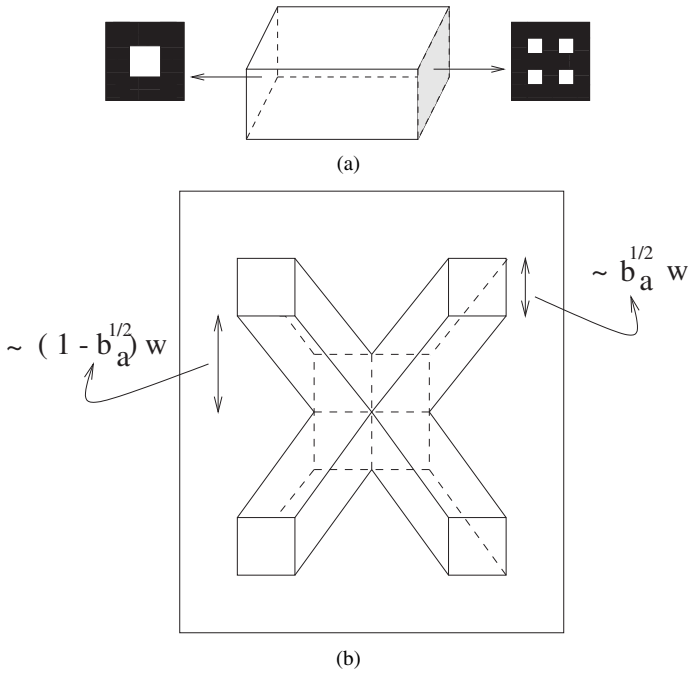


**Fig. 6.** Schematic of the 3D basic cell with dimension $w \times w \times l$: (a) the boundary domain structure; (b) the four normal threads.

The structure is truly three-dimensional, but it still follows our branching algorithm. The basic cell consists of four normal regions (flux threads) in a matrix of superconductor (see Figure 6). Each flux thread branches dyadically as it approaches the faces of the plate.

Our flux tubes have square rather than round cross-sections, because it is easier to write down suitable test fields in this case. Of course isoperimetric effects favor round cross-sections. But the energy scaling law—the main focus of our interest—is insensitive to the choice of cross section. (This is intuitively clear from the following discussion, and rigorously valid as a consequence of Section 5.2.)

**Step 1:** We must specify the structure of the basic cell, which consists of four flux threads (see Figure 6b). We naturally take $\mathbf{B} = 0$ in the superconducting region outside the flux threads. We choose $\mathbf{B}$ constant in each of the four flux threads, with $B_1 = 1$ and $B_2$, $B_3$ chosen so that $\mathbf{B}$ points parallel to the thread wall. Thus the value of $\mathbf{B}$ in the threads is $(1, \pm\lambda, \pm\lambda)$, with

$$\lambda :\cong \frac{(1 - b_a^{1/2})\, w}{l},$$

where the constant is determined by the geometry. The resulting field is weakly divergence-free. The energy $E_{cell}$ of the basic cell satisfies

$$E_{cell} \lesssim \varepsilon\, b_a^{1/2}\, w\, l \;\; + \;\; \lambda^2\, b_a\, w^2\, l \lesssim \varepsilon\, b_a^{1/2}\, w\, l \;\; + \;\; \frac{b_a\, w^4}{l}. \tag{4.6}$$

Optimization in $l$ gives

$$l_{opt}(w) \cong \frac{b_a^{1/4}\, w^{3/2}}{\varepsilon^{1/2}}, \qquad E_{cell} \lesssim \varepsilon^{1/2}\, w^{5/2}\, b_a^{3/4}.$$

**Step 2:** We set $w_m = w/2^m$ and $l_m = l_{opt}(w_m)$. Since there are $1/w^2$ cells that refine, we have

$$E_{inside} \lesssim \frac{1}{w^2} \sum_{m=1}^{\infty} 4^{m-1} \varepsilon^{1/2}\, b_a^{3/4} w^{5/2} \left(\frac{1}{2^m}\right)^{5/2} \lesssim \varepsilon^{1/2}\, w^{1/2}\, b_a^{3/4}.$$

The requirement $l_{opt}(w) \cong L$ gives

$$w \cong \frac{\varepsilon^{1/3}\, L^{2/3}}{b_a^{1/6}} \qquad \text{and} \qquad E_{inside} \lesssim b_a^{2/3}\, \varepsilon^{2/3}\, L^{1/3}. \tag{4.7}$$

Note that $w \lesssim 1$ by (4.5).

**Step 3:** We again use Propositions A.1 and A.2 of the Appendix. The truncation stage $N$ should satisfy

$$E_{outside} \lesssim b_a^{3/2}\, w_N = \frac{b_a^{3/2}\, w}{2^N} \cong b_a^{2/3}\, \varepsilon^{2/3}\, L^{1/3}, \quad \text{whence} \quad w_N \cong \frac{\varepsilon^{2/3}\, L^{1/3}}{b_a^{5/6}}.$$

**Step 4:** We must show that this truncation is admissible. In fact, (4.5) implies

$$\frac{w_N}{l_N} \cong \frac{\varepsilon^{1/6}\, b_a^{1/6}}{L^{1/6}} \lesssim 1 \qquad \text{and} \qquad 2^N \cong \left(\frac{b_a^2\, L}{\varepsilon}\right)^{1/3} \gtrsim 1,$$

so the construction is realizable.

In summary, this 3D branched thread construction shows that

$$\min(\mathcal{P}) \lesssim b_a^{2/3}\, \varepsilon^{2/3}\, L^{1/3},$$

for $b_a \le 1/2$, provided that $\varepsilon$ and $L$ satisfy (4.5).

### *4.4. Thin Tunnels of Superconducting Material—Large Applied Field*

This section presents the large-$b_a$ analogue of Andrews's construction. In this regime we are considering microstructures with a small volume fraction of superconductor. It is no surprise that isoperimetric effects favor superconducting tunnels rather than layers. The details are however quite different from the low-$b_a$ setting, due to the asymmetric roles of the superconducting and normal phases. This construction (and the resulting scaling law) have not, to our knowledge, been previously discussed.

We assume throughout this section that $b_a$ is sufficiently close to 1. The realizability conditions are

$$\frac{\varepsilon^{1/3}\, L^{2/3}}{(1-b_a)^{1/2}\, |\log(1-b_a)|^{1/3}} \lesssim 1 \qquad \text{and} \qquad \varepsilon/L \lesssim |\log(1-b_a)|^{-2}. \tag{4.8}$$

For such $\varepsilon$, $L$, and $b_a$, the construction shows that

$$\min(\mathcal{P}) \lesssim (1-b_a)\,|\log(1-b_a)|^{1/3}\,\varepsilon^{2/3}\,L^{1/3}. \tag{4.9}$$

In its outline, the construction is closely parallel to that of Section 4.3. At scale $w$, the superconducting tunnels have diameter of order $(1-b_a)^{1/2}w$. It is convenient to set

$$\bar{\alpha} = (1-b_a)^{1/2},$$

so $\bar{\alpha}$ plays a role similar to that of $b_a^{1/2}$ in Section 4.3.

Our main task is to specify the basic cell and estimate its energy. Its structure is sketched in Figure 7. The left-hand cross-section has single superconducting circle, while the right-hand cross-section has four superconducting circles. In its interior, the cell has five roughly conical superconducting tunnels in a matrix of normal material. One of these tunnels—the central one—tapers to the right; the others—the peripheral ones—taper to the left. We shall show that this cell can be realized with energy

$$E_{cell} \lesssim \epsilon\,\bar{\alpha}\,w\,l \quad + \quad \bar{\alpha}^4\,|\log\bar{\alpha}|\,\frac{w^4}{l}. \tag{4.10}$$

This formula replaces (4.6) of Section 4.3. Steps 2–4 of the branching algorithm are entirely parallel to those of Section 4.3, except that the admissibility condition (stipulating that the slope of the superconducting-normal interface not be large) is $\bar{\alpha}w_N/l_N \lesssim 1$. Their details can safely be left to the reader.

The rest of this section is devoted to specifying the basic cell, constructing a suitable test field $\mathbf{B}$, and estimating its energy. The hard part is the specification of $\mathbf{B}$. We shall do it in two stages: first giving $\mathbf{B}$ in a (constant cross-section, circular) cylinder around each tunnel; then specifying it in the complement of these cylinders. In determining $\mathbf{B}$ we will focus on a typical cross-section, shown in Figure 8.

We start by specifying more precisely the geometry of the basic cell of size $w \times w \times l$. Let $\theta$ be a sufficiently small constant. Since $b_a$ is close to 1, we may assume that $\bar{\alpha} < \theta$. We take the radius of our cylinders to be

$$r_1 = \theta w.$$

The central superconducting tunnel is approximately conical, tapering to the right, with circular cross-sections. At $0 < x < l$ we take its radius to be

$$r_c(x) := \bar{\alpha} w \phi(x/l), \tag{4.11}$$

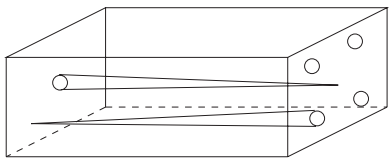

**Fig. 7.** The unit cell: a central superconducting tunnel tapering to the right, and four peripheral superconducting tunnels tapering to the left.

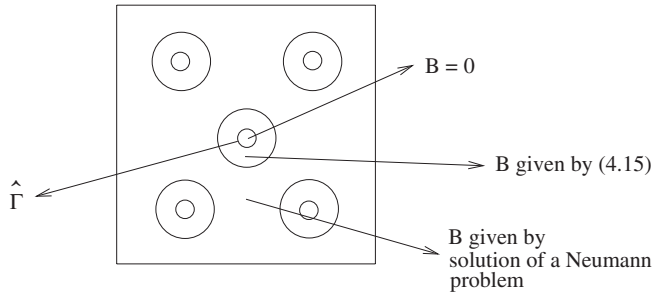


**Fig. 8.** A typical cross-section of the unit cell. The small circles are the superconductor-normal phase boundaries. The larger circles delimit our cylinders. They are not phase boundaries, but we construct **B** separately within and outside of the cylinders.

where $\phi : [0, 1] \to [0, 1]$ is a decreasing function with $\phi(0) = 1$ and $\phi(1) = 0$. The total area of superconductor in each section should be constant. Therefore the four peripheral superconducting tunnels should have cross-sectional radius

$$r_p(x) := \frac{\bar{\alpha}}{2} w[1 - \phi^2(x/l)]^{1/2}. \tag{4.12}$$

We said earlier that the tunnels should be "approximately conical." Actually, what matters is that each be conical near its apex, where **B** is somewhat singular. Therefore we require that for some $\delta > 0$,

$$(1 - \phi^2(t))^{1/2} = t \quad \text{if} \quad 0 \le t \le \delta \qquad \text{and} \qquad \phi(t) = 1 - t \quad \text{if } \delta \le t \le 1. \tag{4.13}$$

It follows that for both the central and peripheral tunnels,

$$\left| \frac{dr}{dx} \right| \lesssim \bar{\alpha} \frac{w}{l}, \quad \text{for } 0 \le x \le l, \tag{4.14}$$

with $r = r_c(x)$ or $r = r_p(x)$.

We turn next to the specification of **B** in the cylinders. Of course $\mathbf{B} = 0$ in each superconducting tunnel, so we have only to give **B** in the region between each tunnel and the associated cylinder boundary. The treatment of the central and peripheral tunnels are similar, so we may focus on the region near the central tunnel. Let $\Gamma$ be the (approximately conical) boundary of the tunnel, and let $\mathbf{n} = (n_1, n_2, n_3)$ be its outward unit normal. At fixed $x$, the cross section of this tunnel is a disk; we denote its boundary by $\hat{\Gamma} = \hat{\Gamma}(x)$. Notice that the in-plane normal to $\hat{\Gamma}$ is $\hat{\mathbf{n}} = (n_2, n_3)/\sqrt{1 - n_1^2}$.

Fixing $x$, we shall take $\mathbf{B} = (1, B_2, B_3)$ in the annular region between the tunnel and the cylinder. Since **B** must be divergence-free as a three-dimensional vector field, we need

$$\partial B_2/\partial y + \partial B_3/\partial z = 0$$

in the annular region, and

$$(B_2, B_3) \cdot \hat{\mathbf{n}} = \frac{-n_1}{\sqrt{1 - n_1^2}}$$

at its inner boundary $\hat{\Gamma}$. Taking $y = z = 0$ to be the center of the annulus and writing $r^2 = y^2 + z^2$, a convenient choice is

$$(B_2, B_3) = A(x)\, r_c(x)\, \left(\frac{y}{r^2}, \frac{z}{r^2}\right), \quad \text{for } r_c(x) < r < r_1, \tag{4.15}$$

with

$$A(x) := \frac{-n_1(x)}{\sqrt{1 - n_1^2(x)}}.$$

Notice that the magnitude of $A(x)$ is controlled:

$$|A(x)| = \left|\frac{dr_c}{dx}\right| \lesssim \bar{\alpha}\, w/l, \tag{4.16}$$

by (4.14). We also note, for later reference, that at the outer boundary $r = r_1$,

$$|(B_2, B_3) \cdot \hat{\mathbf{n}}| = |A(x)|\, \frac{r_c(x)}{r_1} \lesssim \bar{\alpha}^2\, x\, w/l^2 \lesssim \bar{\alpha}^2\, w/l, \tag{4.17}$$

using (4.11), (4.14), and (4.16).

Let us evaluate the magnetic energy associated with the construction thus far. It is

$$\begin{aligned} \int_0^l \int_{\text{annulus}} B_2^2 + B_3^2\, dA\, dx &\lesssim \int_0^l A^2(x)\, r_c^2(x) \int_{r_c(x)}^{r_1} \frac{1}{r^2}\, r\, dr\, dx \\ &\lesssim \int_0^l A^2(x)\, r_c^2(x)\, \log\left(\frac{r_1}{r_c(x)}\right)\, dx. \end{aligned}$$

Using (4.11) and (4.16), we have

$$E_{cylinder} \lesssim \int_0^l \frac{\bar{\alpha}^4 w^4}{l^2} \phi^2\left(\frac{x}{l}\right) \log\left(\frac{\theta}{\bar{\alpha}\, \phi\left(\frac{x}{l}\right)}\right) dx. \tag{4.18}$$

By changing variables to $\bar{x} = x/l$, one easily verifies that the value of this integral is of order $\bar{\alpha}^4 |\log \bar{\alpha}| w^4/l$.

The four peripheral cylinders are handled similarly. Each produces a magnetic energy term of order $\bar{\alpha}^4 |\log \bar{\alpha}| w^4/l$.

It remains to extend $\mathbf{B}$ to the complement of the cylinders. As before, we concentrate on the cross section at fixed $x$ (see Figure 8), and we take $\mathbf{B} = (1, B_2, B_3)$. Our task is now to define $(B_2, B_3)$ in complement of the circles (a square of side $w$, with five circles of radius $\theta w$ removed). It must satisfy

$$\partial B_2/\partial y + \partial B_3/\partial z = 0,$$

with

$$(B_2, B_3) \cdot \hat{\mathbf{n}} = A(x) \frac{r_c(x)}{r_1}$$

at the central circle (to match (4.17)) and a similar condition at each of the four peripheral circles. At the boundary of the square, we can impose either periodicity or the homogeneous condition

$$(B_2, B_3) \cdot \hat{\mathbf{n}} = 0.$$

It is easy to verify that these boundary conditions are compatible (indeed, $(B_2, B_3) \cdot \hat{\mathbf{n}}$ averages to 0 around each circle separately; see e.g. (4.15)). A convenient choice is obtained by solving Laplace's equation $\Delta\psi = 0$, with inhomogeneous Neumann data at each circle and homogeneous Neumann data at the boundary of the square, then taking

$$(B_2, B_3) = \left( \frac{\partial \psi}{\partial y}, \frac{\partial \psi}{\partial z} \right).$$

This PDE is being solved in a *fixed* domain (independent of $x$, and even independent of $w$ after scaling); the Neumann data depend on $x$ but are uniformly bounded, according to (4.17), by a constant times $\bar{\alpha}^2\, w/l$. By an elementary elliptic estimate, the solution satisfies a bound of the same order:

$$\left( \frac{1}{w^2} \int |\nabla \psi(y, z)|^2 \, dy \, dz \right)^{1/2} \lesssim \bar{\alpha}^2\, w/l.$$

Thus the magnetic energy outside the cylinders is

$$\int B_2^2 + B_3^2 \, dy \, dz \, dx \lesssim \left( \frac{\bar{\alpha}^2\, w}{l} \right)^2 w^2 l = \frac{\bar{\alpha}^4\, w^4}{l}.$$

The desired estimate (4.10) follows immediately from this result, (4.18), and elementary geometry.

### 4.5. *Clusters of Branched Normal Threads: A Two-Scale Construction for the Smallest Applied Fields*

The constructions in Sections 4.3 and 4.4 have a certain uniformity. The flux threads (for low $b_a$) or superconducting tunnels (for high $b_a$) are distributed uniformly in the $(y, z)$ directions, in the sense that they intersect each plane $x =$ constant in a periodic pattern. The threads or tunnels refine by a sort of branching process as they approach the faces $x = 0, L$. The branching creates additional surface and magnetic energy within the plate, but it reduces the external magnetic energy. As a result it leads to an $\varepsilon^{2/3} L^{1/3}$ scaling law, better than the $\varepsilon^{1/2} L^{1/2}$ scaling achieved without branching—except perhaps near $b_a = 0$ or 1, when the prefactor is important.

This section presents a different, less uniform construction, which does better when $b_a$ is small enough. The idea is simple: We let the flux tubes branch, but we keep them in relatively small bundles. Compared with the uniform branching of Section 4.3, this saves interior magnetic energy, since the tubes stay more nearly parallel to the $x$-axis; but it costs exterior magnetic energy, since the pattern on the faces $x = 0, L$ has a larger length scale. The construction is realizable if

$$\varepsilon^{3/7} L^{4/7} \lesssim b_a^{1/2} \qquad \text{and} \qquad b_a^{7/2} \lesssim \varepsilon/L \lesssim 1; \tag{4.19}$$

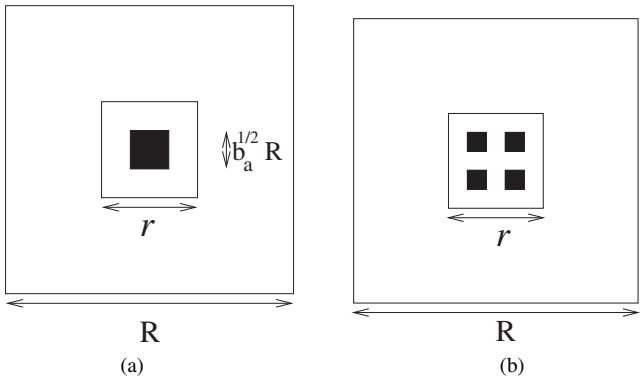


**Fig. 9.** The two-scale construction: (a) a section in the middle of the plate showing the two scales $R$ and $r$; (b) a section closer to the face of the plate, after one generation of refinement. Note that, contrary to our prior convention, the normal regions are now black.

in this regime it shows that

$$\min(\mathcal{P}) \lesssim b_a \varepsilon^{4/7} L^{3/7}. \tag{4.20}$$

Notice that the hypothesis $b_a^{7/2} \lesssim \varepsilon/L$ is exactly the condition that this construction does better than the one in Section 4.3, i.e. the condition that $b_a \varepsilon^{4/7} L^{3/7} \lesssim b_a^{2/3} \varepsilon^{2/3} L^{1/3}$.

The hard work has already been done in Steps 1 and 2 of Section 4.3. There we constructed, for any $w$ and any $b < 1/2$, a pattern of branching normal threads in the cylinder $(0, L) \times (0, w) \times (0, w)$ with volume fraction $b$ of normal material and $1 - b$ of superconductor. The internal energy of this pattern is, from Section 4.3,

$$\int_0^L \int_0^w \int_0^w \varepsilon |\nabla \chi| + [B_2^2 + B_3^2 + (1 - \chi)(B_1 - 1)^2]\, dx\, dy\, dz \lesssim b^{3/4} \varepsilon^{1/2} w^{5/2}. \tag{4.21}$$

The branching must stop after finitely many steps, say $N$, due to the condition that $w_N \lesssim l_N = l_{opt}(w_N) \cong b^{1/4} w_N^{3/2} \varepsilon^{-1/2}$. This gives the condition

$$w_N \gtrsim b^{-1/2} \varepsilon. \tag{4.22}$$

We also need $\sum_m l_m \cong L$; since this is a geometric series, the condition is equivalent to

$$b^{1/4} w^{3/2} \varepsilon^{-1/2} \cong L. \tag{4.23}$$

Our two-scale construction is shown schematically in Figure 9. The period cell $Q = (0, 1)^2$ is divided into squares of side $R$; at the center of each square lies a flux thread bundle of side $r$ and volume fraction $b_a R^2/r^2$. To evaluate the interior (surface + magnetic) energy, we apply (4.21) with $w$ replaced by $r$ and $b$ replaced by $b_a R^2/r^2$, then sum a geometric series; this gives

$$E_{interior} \lesssim R^{-2} \cdot \left( \frac{b_a R^2}{r^2} \right)^{3/4} \varepsilon^{1/2} r^{5/2} = \varepsilon^{1/2} b_a^{3/4} R^{-1/2} r. \tag{4.24}$$

Now, $r$ and $R$ are not independent: They are coupled by (4.23) with $w$ replaced by $r$ and $b$ replaced by $b_a R^2/r^2$. This gives after simplification

$$R \cong L^2 \varepsilon r^{-2} b_a^{-1/2}, \tag{4.25}$$

and substitution into (4.24) gives

$$E_{interior} \lesssim b_a r^2 L^{-1}. \tag{4.26}$$

To estimate the exterior energy, we observe that at the faces $x = 0, L$ the form of $B_1 = f(y, z)$ is a doubly periodic function with period $R$, which on each $R \times R$ period-square is given by

$$f = \begin{cases} 1 & \text{on little squares occupying area fraction } b_a R^2/r^2 \text{ on an interior} \\ & r \times r \text{ square, arranged periodically at scale } w_N, \\ 0 & \text{on the rest of the } r \times r \text{ square,} \\ 0 & \text{outside the } r \times r \text{ square.} \end{cases}$$

It is convenient to compare this with the function obtained by averaging over each $r \times r$ square:

$$\bar{f} = \begin{cases} b_a R^2/r^2 & \text{on each } r \times r \text{ square,} \\ 0 & \text{outside the } r \times r \text{ squares,} \end{cases}$$

on each $R \times R$ period-square. By the triangle inequality and the definition of the $H^{-1/2}$ norm, we have

$$E_{exterior} \lesssim \left( \|f - \bar{f}\|_{H^{-1/2}} + \|\bar{f} - b_a\|_{H^{-1/2}} \right)^2.$$

Applying Proposition A.2 from the Appendix with $\alpha = r^2/R^2$ and $m = 1/R$, we obtain

$$\|\bar{f} - b_a\|_{H^{-1/2}}^2 \lesssim (b_a R^2/r^2)^2 (r^2/R^2)^{3/2} R = b_a^2 R^2 r^{-1}. \tag{4.27}$$

We claim that similar arguments, which we will address at the end of this section, lead to

$$\|f - \bar{f}\|_{H^{-1/2}}^2 \lesssim (b_a R^2/r^2)^{3/2} w_N (r^2/R^2) = b_a^{3/2} w_N R r^{-1}. \tag{4.28}$$

The former is dominant, i.e. $\|f - \bar{f}\|_{H^{-1/2}}^2 \lesssim \|\bar{f} - b_a\|_{H^{-1/2}}^2$, if $w_N$ is small enough, specifically if

$$w_N \lesssim b_a^{1/2} R. \tag{4.29}$$

Under this hypothesis the exterior energy is $b_a^2 R^2 r^{-1}$ and the total energy is thus

$$E_{total} \lesssim b_a r^2 L^{-1} + b_a^2 R^2 r^{-1} \cong b_a r^2 L^{-1} + b_a \varepsilon^2 r^{-5} L^4.$$

Optimizing over $r$ gives

$$r \cong \varepsilon^{2/7} L^{5/7} \qquad \text{and} \qquad E_{total} \lesssim b_a \varepsilon^{4/7} L^{3/7},$$

which is the desired estimate.

It remains to check feasibility. We require

(a) $r \lesssim R \lesssim 1$ and $b_a R^2/r^2 \lesssim 1$, so the construction makes geometric sense; and
(b) $(b_a R^2/r^2)^{-1/2}\varepsilon \lesssim b_a^{1/2} R$ so $w_N$ can be chosen to satisfy both (4.22) and (4.29)—in other words, so the termination of refinement dictated by (4.22) does not contribute significantly to the exterior energy.

One easily verifies that these conditions are satisfied in the regime (4.19).

Lastly we address (4.28). Using Proposition A.2 of the appendix, it follows that

$$\|f - \bar{f}\|^2_{H^{-1/2}} = R\,\|g\|^2_{H^{-1/2}}, \tag{4.30}$$

where $g$ is defined on the unit cube $Q$ by

$$g = \begin{cases} 1 - b_a \frac{R^2}{r^2} & \text{on little squares occupying area fraction } b_a R^2/r^2 \text{ of one} \\ & \text{interior } r/R \times r/R \text{ square, arranged periodically at scale } w_N/R, \\ -b_a \frac{R^2}{r^2} & \text{on the rest of the } r/R \times r/R \text{ square,} \\ 0 & \text{outside the } r/R \times r/R \text{ square.} \end{cases}$$

Proposition A.1 of the appendix shows how to relate the $H^{-1/2}$ norm squared to the $L^2$ norm squared of a "fringe field" $\nabla u$ which lives outside the sample. There we use periodic boundary conditions in $y$ and $z$ but because of the symmetry of $g$, using instead Neumann boundary conditions ($\nabla u \cdot n = 0$) leads to the exact same solution; the Fourier decompositions of $g$, hence $u$, involve only the cosine eigenfunctions. Hence to calculate the fringe field $u$ associated with $g$, it suffices to construct the fringe field associated with the internal $r/R \times r/R$ square using the Neumann boundary conditions (in $y$, $z$), and then extend with 0 outside the internal cubic cylinder. Moreover, by symmetry, we may compute the $L^2$ norm squared of this internal fringe field by the value of the $H^{-1/2}$ norm squared from Proposition A.2 applied to the periodic extension,[1] and then discount appropriately with the volume fraction $(r/R)^2$. To this end, we consider $Q$ containing a periodic array of $r/R \times r/R$ squares, each with internal structure of the interior part of $g$. By Proposition A.2, the associated $H^{-1/2}$ norm squared is

$$\left(b_a \frac{R^2}{r^2}\right)^{3/2} \frac{w_N}{R}.$$

Combining this with (4.30), we have

$$\|f - \bar{f}\|^2_{H^{-1/2}} \lesssim R \left(b_a \frac{R^2}{r^2}\right)^{3/2} \frac{w_N}{R}\,\frac{r^2}{R^2} = b_a^{3/2}\,\frac{w_N R}{r}.$$

[1] Here we are applying the $H^{-1/2}$ norm to a function that does not have mean value zero. This is only an issue of definition; we may just as well have defined the $H^{-1/2}$ norm on equivalence classes of functions where two functions are equivalent if they differ by a constant.

## 5. Supporting the Guesses: Local Optimality of the Constructions

The constructions in Section 4 give upper bounds on the minimum energy. Here and in Section 7 we shall give corresponding lower bounds.

Our immediate goal is relatively modest. For the constructions in Section 4, which involve a basic unit cell and dyadic branching, we wish to show that the basic unit cells were chosen well and the magnetic energy was estimated efficiently. This is the impact of Section 5.2. The match between bounds and constructions is perfect for the cells used in Sections 4.1 to 4.3; it misses by a logarithmic factor for the cells of Section 4.4.

In truth, however, we also have a more ambitious goal. Section 5.1 develops a flexible method for bounding the magnetic energy from below. The importance of this result goes far beyond the specific application in Section 5.2: It motivates our analysis of the "toy problems" in Section 6. And it is this approach, not the one of Section 7, that achieves the optimal scaling laws for $b_a$ near 0 or 1, as we shall explain in [12].

### *5.1. A Lower Bound on the Magnetic Energy, for Fixed End Conditions*

The basic unit cells in Sections 4.1 to 4.4 were choices of $\mathbf{B}$ and $\chi$, defined for $x$ in some interval $0 < x < l$ and $Q$-periodic in $y$ and $z$. It is easy to see (using that $\operatorname{div}\mathbf{B} = 0$) that if the bulk energy

$$\int_0^l \int_Q \left[B_2^2 + B_3^2 + (1-\chi)(B_1 - 1)^2\right] dx\, dy\, dz$$

vanishes, then $B_1$ must be independent of $x$. So it is natural to seek a lower bound for the bulk energy in terms of the difference between $B_1$ at the two ends of the cell, $x = 0$ and $x = l$. The following proposition achieves such a bound.

**Proposition 5.1.** *Consider any divergence-free vector field* $\mathbf{B}$ *and characteristic function* $\chi$*, defined for* $0 < x < l$ *and* $Q$*-periodic in* $y$ *and* $z$*, with* $\mathbf{B}\chi = 0$*. Let*

$$b = \int_Q B_1(x, y, z)\, dy\, dz, \tag{5.1}$$

*noting that the right-hand side is independent of* $x$ *(Lemma 3.1). Define*

$$\mathcal{L} = \max\left\{\int_Q [B_1(l, y, z) - B_1(0, y, z)]\, g(y, z)\, dy\, dz : \right.$$
$$\left. g \text{ periodic, Lipschitz continuous, } |\nabla g| \le 1\right\}, \tag{5.2}$$

*and assume that*

$$\frac{\mathcal{L}}{lb} \lesssim 1. \tag{5.3}$$

*Then*

$$\int_0^l \int_Q \left[B_2^2 + B_3^2 + (1-\chi)(B_1 - 1)^2\right] dx\, dy\, dz \gtrsim \frac{\mathcal{L}^2}{bl}. \tag{5.4}$$

*Proof.* The idea of the proof is this. If we ignore surface energy, then the minimum magnetic energy consistent with specified boundary conditions is described by the relaxed problem discussed in Section 2.1. Since the relaxed problem is convex, its dual provides a natural framework for proving lower bounds. (These comments are offered purely for motivation. As usual when using duality, the argument is finally elementary—making no explicit use of convexity or relaxation.)

Our starting point is the relation

$$B_2^2 + B_3^2 + (1-\chi)(B_1-1)^2 \geq 2|\mathbf{B}| - 2B_1. \tag{5.5}$$

The proof is elementary: Where $\chi = 1$ both sides vanish, and where $\chi = 0$ we have

$$B_2^2 + B_3^2 + (B_1-1)^2 = 1 + |\mathbf{B}|^2 - 2B_1 \geq 2|\mathbf{B}| - 2B_1.$$

Applying (5.5), we see that for any Lipschitz continuous $u(x, y, z)$ with $|\nabla u| \leq 1$,

$$\int_0^l \int_Q \left[B_2^2+B_3^2+(1-\chi)(B_1-1)^2\right] dx\, dy\, dz \geq 2\int_0^l \int_Q [\langle \mathbf{B}, \nabla u\rangle - B_1]\, dx\, dy\, dz. \tag{5.6}$$

Now consider the choice

$$u(x, y, z) = (1+\gamma^2)^{-1/2}(x + \gamma g(y, z)),$$

where $g$ is periodic and Lipschitz continuous with $|\nabla g| \leq 1$ and $\gamma > 0$ is an arbitrary constant. Since $\mathbf{B}$ is $Q$-periodic with $\operatorname{div} \mathbf{B} = 0$, an easy integration by parts gives

$$\begin{aligned}
&\int_0^l \int_Q \langle \mathbf{B}, \nabla u\rangle\, dx\, dy\, dz \\
&\qquad = \int_0^l \int_Q \frac{\partial}{\partial x}(B_1 u)\, dx\, dy\, dz \\
&\qquad = \int_Q [B_1(l, y, z)u(l, y, z) - B_1(0, y, z)u(0, y, z)]\, dy\, dz \\
&\qquad = (1+\gamma^2)^{-1/2}\left\{ lb + \gamma \int_Q [B_1(l, y, z) - B_1(0, y, z)]\, g(y, z)\, dy\, dz \right\}.
\end{aligned}$$

Since $\int_0^l \int_Q B_1\, dx\, dy\, dz = bl$, we conclude after maximization over $g$ that

$$\frac{1}{2}\int_0^l \int_Q B_2^2+B_3^2+(1-\chi)(B_1-1)^2\, dx\, dy\, dz \geq [(1+\gamma^2)^{-1/2}-1]lb+\gamma(1+\gamma^2)^{-1/2}\mathcal{L}.$$

For any $\gamma$ we have $(1+\gamma^2)^{-1/2}-1 \geq -\frac{1}{2}\gamma^2$, and for $0 \leq \gamma \leq 1$ we have $\gamma(1+\gamma^2)^{-1/2} \geq \gamma/\sqrt{2}$. Using these inequalities, our lower bound becomes

$$-\tfrac{1}{2}\gamma^2 lb + \frac{1}{\sqrt{2}}\gamma\mathcal{L}. \tag{5.7}$$

Let $c_0$ be the constant implicit in (5.3), i.e. suppose

$$\frac{\mathcal{L}}{lb} \leq c_0.$$

Then a convenient choice is

$$\gamma = \frac{\mathcal{L}}{c_1 lb} \qquad \text{with } c_1 = \max\{c_0, 1\}.$$

Clearly $0 \le \gamma \le 1$, and substitution in (5.7) gives

$$\left(-\frac{1}{2c_1} + \frac{1}{\sqrt{2}}\right)\frac{\mathcal{L}^2}{c_1 lb} \gtrsim \frac{\mathcal{L}^2}{lb},$$

since $c_1 \ge 1$. So our lower bound becomes

$$\int_0^l \int_Q B_2^2 + B_3^2 + (1-\chi)(B_1 - 1)^2 \, dx\, dy\, dz \gtrsim \frac{\mathcal{L}^2}{lb}, \tag{5.8}$$

which is the desired result. □

*Remark.* We note that $\mathcal{L}$, defined by (5.2), is (by definition) the Monge-Kantorovich norm of $B_1(l, y, z) - B_1(0, y, z)$. Since $B_1$ prefers to be 1 in the normal material while $B_1$ must be 0 in the superconductor, $\mathcal{L}$ is roughly the Monge-Kantorovich norm of the difference between the characteristic functions $\chi(l, y, z)$ and $\chi(0, y, z)$ representing the phase geometry at the two ends $x = 0, l$. It has the dimensions of length and provides a measure of the "physical scale" on which the difference $\chi(l, y, z) - \chi(0, y, z)$ oscillates.

The proof of Proposition 5.1 actually achieves somewhat more than the assertion of the proposition. Indeed, the argument is not restricted to the $g$ that maximizes (5.2), and this will be important below. We have shown

**Corollary 5.2.** *Suppose $g(y, z)$ is Lipschitz continuous and periodic on $Q$, with $|\nabla g| \le 1$ pointwise. Let*

$$\mathcal{L}_1 = \int_Q [B_1(l, y, z) - B_1(0, y, z)]\, g(y, z)\, dy\, dz,$$

*and assume that*

$$\frac{\mathcal{L}_1}{lb} \lesssim 1.$$

*Then we have the following lower bound for the bulk energy:*

$$\int_0^l \int_Q \left[B_2^2 + B_3^2 + (1-\chi)(B_1 - 1)^2\right] dx\, dy\, dz \gtrsim \frac{\mathcal{L}_1^2}{bl}.$$

### *5.2. Optimal Scaling of the Unit Cells*

We now apply Corollary 5.2 to show that the basic unit cells of Sections 4.1 to 4.3 achieve the optimal scaling laws. We will also show that the cell of Section 4.4 misses the optimal scaling by at most a logarithmic factor.

Consider first the branched, layered construction presented in Sections 4.1 and 4.2. Its basic unit cell is shown in Figures 4 and 5. When the length is $l$ and the width is $w$, its bulk energy is

$$\int_0^l \int_{-w/2}^{w/2} \left[B_2^2 + (1-\chi)(B_1-1)^2\right] dx\, dy \sim (1-b_a)^2 b_a \frac{w^3}{l};$$

this was a crucial ingredient for Step 1 of our branching algorithm. Periodic extension in $y$ gives a choice of $\mathbf{B}$ and $\chi$ defined in the entire cylinder $(0,l)\times Q$ (independent of $z$ and satisfying $B_3 = 0$) with bulk energy

$$\int_0^l \int_Q \left[B_2^2 + B_3^2 + (1-\chi)(B_1-1)^2\right] dx dy dz \sim \begin{cases} b_a w^2 l^{-1} & \text{for } b_a \text{ near } 0, \\ (1-b_a)^2 w^2 l^{-1} & \text{for } b_a \text{ near } 1. \end{cases} \tag{5.9}$$

We claim that no other choice with the same end conditions at $x = 0, l$ can achieve a better scaling law.

Consider first the case when $b_a$ is near 0. Then $B_1(l,y) - B_1(0,y)$ has the form $\phi(y/w)$, where $\phi$ is periodic with period 1 and mean value 0. Since $b_a$ is small, $\phi$ takes the values $\pm 1$ on short intervals (each having length of order $b_a$), and it equals 0 off these intervals. So one easily constructs a function $g(y)$, periodic with period 1, such that $|g'| \le 1$ and $\int_0^1 \phi(y) g(y)\, dy \sim b_a$. Using the notation of Corollary 5.2 with test function $g_w(y) = w g(y/w)$, we find that

$$\mathcal{L}_1 =: \int_0^1 \phi(y/w) g_w(y)\, dy \sim w b_a.$$

The corollary applies if $\mathcal{L}_1/(l b_a) \lesssim 1$, i.e. if $w/l$ is at most of order one, and it gives the lower bound

$$\int_0^l \int_Q \left[B_2^2 + B_3^2 + (1-\chi)(B_1-1)^2\right] dx\, dy\, dz \gtrsim b_a w^2 l^{-1}.$$

This matches (5.9), verifying the optimality of our 2D unit cell in the low-$b_a$ regime.

The argument for $b_a$ near 1, is only slightly different. We still have $B_1(l,y) - B_1(0,y) = \phi(y/w)$ with $\phi$ periodic of period 1. But for $b_a$ near 1, $\phi$ takes the values $\pm 1$ on short intervals each having length of order $1 - b_a$, and it equals 0 elsewhere. Arguing as above, we get (for a suitable $g$)

$$\mathcal{L}_1 = \int_0^1 \phi(y/w) g_w(y)\, dy \sim w(1-b_a).$$

Corollary 5.2 applies if $\mathcal{L}_1/(l b_a) \lesssim 1$; for $b_a$ near 1, this requires that $w(1-b_a)/l$ be at most of order one. The conclusion of the corollary is

$$\int_0^l \int_Q \left[B_2^2 + B_3^2 + (1-\chi)(B_1-1)^2\right] dx\, dy\, dz \gtrsim (1-b_a)^2 w^2 l^{-1},$$

which matches (5.9), verifying the optimality of our 2D unit cell in the high-$b_a$ regime.

We turn now to the 3D, small-applied-field construction presented in Section 4.3. Its basic unit cell, shown in Figure 6, has thin threads of normal material in a matrix of superconductor. When the length is $l$ and the width is $w$, its bulk energy is

$$\int_0^l \int_{-w/2}^{w/2} \int_{-w/2}^{w/2} \left[B_2^2 + B_3^2 + (1-\chi)(B_1-1)^2\right] dx\, dy\, dz \sim b_a \frac{w^4}{l};$$

we used this fact in Section 4.3. Periodic extension gives a $\mathbf{B}$ and $\chi$ defined in the entire cylinder $(0, l) \times Q$ with bulk energy

$$\int_0^l \int_Q \left[B_2^2 + B_3^2 + (1-\chi)(B_1-1)^2\right] dx\, dy\, dz \sim b_a \frac{w^2}{l}. \tag{5.10}$$

The argument leading to a matching lower bound is much as before: $B_1(l, y, z) - B_1(0, y, z)$ has the form $\phi(\frac{y}{w}, \frac{z}{w})$ where $\phi$ is periodic with period 1 and mean value 0. Now $\phi$ takes the values $\pm 1$ on small squares, each having area of order $b_a$; off these squares it equals 0. One easily constructs a function $g(y, z)$, periodic with period 1, such that $|\nabla g| \le 1$ and $\int_Q \phi(y, z)\, g(y, z)\, dy dz \sim b_a$. Using the test function $g_w(y, z) = w g\left(\frac{y}{w}, \frac{z}{w}\right)$, we get

$$\mathcal{L}_1 = \int_Q \phi\left(\frac{y}{w}, \frac{z}{w}\right) g_w(y, z)\, dy\, dz \sim w b_a.$$

Corollary 5.2 applies for $w/l \lesssim 1$, and it gives the lower bound

$$\int_0^l \int_Q \left[B_2^2 + B_3^2 + (1-\chi)(B_1-1)^2\right] dx\, dy\, dz \gtrsim b_a w^2 l^{-1},$$

which matches (5.10).

Finally we turn to the 3D, large-applied-field construction presented in Section 4.4. Its basic unit cell, shown in Figure 7, has thin tunnels of superconductor in a matrix of normal material. When the length is $l$ and the width is $w$, its bulk energy is

$$\int_0^l \int_{w/2}^{w/2} \int_{w/2}^{w/2} \left[B_2^2 + B_3^2 + (1-\chi)(B_1-1)^2\right] dx\, dy\, dz \sim (1-b_a)^2 |\log(1-b_a)| \frac{w^4}{l};$$

we used this fact in Section 4.4. Periodic extension gives a $\mathbf{B}$ and $\chi$ defined in the entire cylinder $(0, l) \times Q$ with bulk energy

$$\int_0^l \int_Q \left[B_2^2 + B_3^2 + (1-\chi)(B_1-1)^2\right] dx\, dy\, dz \sim (1-b_a)^2 \log|(1-b_a)| \frac{w^2}{l}. \tag{5.11}$$

This is the one regime where our lower bound does not match the construction—it lacks the logarithmic factor. The argument is similar to the other cases. We still have

$B_1(l, y, z) - B_1(0, y, z) = \phi(y/w, z/w)$, where $\phi$ is periodic with period 1 and mean value 0. This time $\phi$ takes the values $\pm 1$ on small disks, each having area of order $1 - b_a$, and it equals 0 elsewhere. Arguing as usual, we get $\mathcal{L}_1 \sim w(1 - b_a)$. Corollary 5.2 applies if $\mathcal{L}_1/(lb_a) \lesssim 1$; for $b_a$ near 1, this requires $w(1 - b_a)/l \lesssim 1$. The conclusion of the corollary is

$$\int_0^l \int_Q \left[B_2^2 + B_3^2 + (1 - \chi)(B_1 - 1)^2\right] dx\, dy\, dz \gtrsim (1 - b_a)^2 w^2 l^{-1}, \tag{5.12}$$

which lacks the logarithmic factor of (5.11).

It is natural to wonder which is suboptimal: the construction in Section 4.4 or the lower bound (5.12). We will show in the upcoming paper [12] that this bound is suboptimal, i.e. the logarithmic factor is necessarily present.

*Remark.* The constructions in Section 4 made many geometric choices. Focusing for example on the 3D small-applied-field setting, we chose the cross section of the normal threads to be rectangular; we decided that one tube should branch into four in the basic unit cell; and we chose the geometry of that branching. We did not attempt to optimize over such geometric choices, because optimization seemed unlikely to change the scaling law. Our lower bounds confirm the insensitivity of the scaling law to these geometric choices. Indeed, the bounds are very robust. Their scaling depends mainly on the periodicity of the cross sections, not on the details of the phase geometry.

## 6. Toy Problems for the Local Length Scale

We now revisit the constructions of Sections 4.1 to 4.4. They have a lot in common, differing mainly in the choice of cross-sectional geometry, so it is natural to seek a unified viewpoint. The "toy problems" presented here achieve this goal, as well as considerable simplification.

Each toy problem is a one-dimensional variational problem for the local length scale $h(x)$ at depth $0 \le x \le L$. Its terms represent surface energy, interior magnetic energy, and exterior magnetic energy. The expressions for these terms reflect the underlying geometric choices (e.g. lamellar versus 3D branching), and they capture the asymmetry between $b_a \to 0$ and $b_a \to 1$.

We find the toy problems enlightening because they capture the essential physics of the constructions while avoiding the tedious geometrical details. In particular they explain the energy scaling laws: Each is an immediate consequence of the associated toy problem after nondimensionalization. A similar argument was used long ago by Hubert to explain the scaling of magnetic domains in a uniaxial ferromagnet [21].

To formulate a toy problem, one must fix in advance the overall geometry of the construction, leaving a single local length scale $h(x)$ to be determined. The two-scale construction of Section 4.5 does not fit this mold, since it has two distinct length scales. Therefore we do not offer a toy problem for that case.

### *6.1. Lamellar Structures*

We first address the 2D (lamellar) structures considered in Sections 4.1 and 4.2. We claim the essential physics is captured (for both large and small $b_a$) by the toy problem

$$(\mathcal{TP})_1 \quad \min_{h(x)} \left\{ \int_0^L \left[ \frac{\varepsilon}{h(x)} + (1-b_a)^2 b_a h_x^2 \right] dx + \psi(b_a)\, h(0) + \psi(b_a)\, h(L) \right\},$$

where $\psi(b_a)$ is of order 1 for $b_a$ bounded away from 0 and 1, and

$$\psi \sim b_a^2 \,|\log(b_a)| \quad \text{for } b_a \to 0, \qquad \psi \sim (1-b_a)^2 \,|\log(1-b_a)| \quad \text{for } b_a \to 1.$$

The integral of $\varepsilon/h(x)$ represents surface energy. The terms $\psi(b_a)h(0)$ and $\psi(b_a)h(L)$ represent exterior magnetic energy, evaluated using Propositions A.1 and A.2 of the appendix. These need no explanation—they are dictated by the lamellar geometry.

The middle term represents the interior magnetic energy associated with changes in the length scale $h$. To explain its form, consider a sequence $x_1 < x_2 < \cdots$ such that $h(x_{i+1}) = h(x_i)/2$. According to Section 5.2—see (5.9) and the argument just following it—the magnetic energy between $x_i$ and $x_{i+1}$ is of order

$$(1-b_a)^2 b_a \frac{h^2(x_i)}{x_{i+1}-x_i}.$$

Since our choice of $x_i$ gives $h(x_i) - h(x_{i+1}) = h(x_i)/2$, this is a constant times

$$(1-b_a)^2 b_a \frac{(h(x_{i+1}) - h(x_i))^2}{x_{i+1}-x_i}.$$

In formulating $(\mathcal{TP})_1$ we have approximated this expression by

$$(1-b_a)^2 b_a \int_{x_i}^{x_{i+1}} h_x^2 \, dx,$$

and summed over $i$.

Let us nondimensionalize $(\mathcal{TP})_1$. Our branched construction predicts that the length scale in the center of the sample is of order $\varepsilon^{1/3} L^{2/3} b_a^{-1/3} (1-b_a)^{-2/3}$ (see (4.2)). Letting $D_L$ denote this length, consider the nondimensional quantities $\bar{h}$ and $\bar{x}$ defined by

$$\bar{x} = \frac{x}{L}, \qquad \bar{h}(\bar{x}) = \frac{1}{D_L} h(x).$$

In the new variables, $(\mathcal{TP})_1$ becomes

$$(\mathcal{NDTP})_1 \quad \varepsilon^{2/3} L^{1/3} b_a^{1/3} (1-b_a)^{2/3} \cdot \min_{\bar{h}(\bar{x})} \left\{ \int_0^1 \left[ \frac{1}{\bar{h}(\bar{x})} + \bar{h}_{\bar{x}}^2 \right] d\bar{x} + \gamma_1 \bar{h}(0) + \gamma_1 \bar{h}(1) \right\},$$

with

$$\gamma_1 = \left( \frac{L}{\varepsilon} \right)^{1/3} \frac{\psi(b_a)}{b_a^{2/3} (1-b_a)^{4/3}}.$$

We shall show in Section 6.4 that, for $\gamma_1 \gtrsim 1$, the expression in braces is of order 1. We thus recover the main conclusions of Sections 4.1 and 4.2: The energy scaling law for the 2D (laminar) construction is $b_a^{1/3}(1-b_a)^{2/3}\varepsilon^{2/3}L^{1/3}$.

### *6.2. Normal Threads*

We now address the construction of Section 4.3, involving a small volume fraction of normal threads. We assume $b_a \leq 1/2$, and write $\alpha = b_a^{1/2}$ for notational convenience. We claim the essential physics is captured by the toy problem

$$(\mathcal{TP})_2 \qquad \min_{h(x)} \left\{ \int_0^L \left[ \frac{\alpha\,\varepsilon}{h(x)} + \alpha^2\, h_x^2 \right] dx + \alpha^3\, h(0) + \alpha^3 h(L) \right\}.$$

The first term under the integral is the surface energy. It is proportional to the surface area of the threads—hence the factor of $\alpha$. The second term under the integral is the interior magnetic energy, estimated as in Section 6.1 but using (5.10) in place of (5.9). The terms $\alpha^3 h(0)$ and $\alpha^3 h(L)$ represent external magnetic energy, evaluated once again using Propositions A.1 and A.2 of the Appendix.

We nondimensionalize. Our branched constructions predict that the length scale in the middle of the plate is of order $\varepsilon^{1/3}\, L^{2/3}\, \alpha^{-1/3}$. Letting $D_L$ denote this length and defining the nondimensional quantities $\bar{h}$ and $\bar{x}$ as before, $(\mathcal{TP})_2$ becomes

$$(\mathcal{NDTP})_2 \qquad \varepsilon^{2/3}\, L^{1/3}\, b_a^{2/3} \cdot \min_{\bar{h}(\bar{x})} \left\{ \int_0^1 \left[ \frac{1}{\bar{h}(\bar{x})} + \bar{h}_{\bar{x}}^2 \right] d\bar{x} + \gamma_2\, \bar{h}(0) + \gamma_2\, \bar{h}(1) \right\},$$

with

$$\gamma_2 = \left( \frac{L}{\varepsilon} \right)^{1/3} b_a^{2/3}.$$

We thus recover the main conclusion of Section 4.3: For $\gamma_2 \gtrsim 1$, the energy scaling law of this construction is $b_a^{2/3} \varepsilon^{2/3} L^{1/3}$.

### *6.3. Superconducting Tunnels*

Finally, we address the construction of Section 4.4, involving a small volume fraction of superconducting tunnels. We assume $1 - b_a$ is sufficiently small, and write $\bar{\alpha} = (1 - b_a)^{1/2}$ for notational convenience. We claim the essential physics is captured by the toy problem

$$(\mathcal{TP})_3 \qquad \min_{h(x)} \left\{ \int_0^L \left[ \frac{\bar{\alpha}\,\varepsilon}{h(x)} + \bar{\alpha}^4\, |\log(\bar{\alpha})|\, h_x^2 \right] dx + \bar{\alpha}^3\, h(0) + \bar{\alpha}^3\, h(L) \right\}.$$

The explanation is much as before. The justification of the term representing interior magnetic energy follows the argument in Section 6.1 with (5.9) replaced by (5.11). (We use (5.11) not (5.12) because we know, from recent work [12], that it is the construction that is optimal, not the lower bound (5.12).)

We nondimensionalize as before. For the construction of Section 4.4, the length scale at the center of the plate is

$$D_L = \frac{\varepsilon^{1/3} L^{2/3}}{\bar{\alpha} |\log \bar{\alpha}|^{1/3}}.$$

Defining $\bar{h}$ and $\bar{x}$ as usual, $(\mathcal{TP})_3$ becomes

$$(\mathcal{NDTP})_3 \qquad \varepsilon^{2/3} L^{1/3} (1 - b_a) |\log(1 - b_a)|^{1/3} \cdot \min_{\bar{h}(\bar{x})} \left\{ \int_0^1 \left[ \frac{1}{\bar{h}(\bar{x})} + \bar{h}_{\bar{x}}^2 \right] d\bar{x} + \gamma_3 \bar{h}(0) + \gamma_3 \bar{h}(1) \right\},$$

with

$$\gamma_3 = \left( \frac{L}{\varepsilon |\log(1 - b_a)|^2} \right)^{1/3}.$$

We thus recover the main conclusion of Section 4.4: For $\gamma_3 \gtrsim 1$, the energy scaling law of this construction is $\varepsilon^{2/3} L^{1/3} (1 - b_a) |\log(1 - b_a)|^{1/3}$.

### *6.4. Toy Problem Predictions*

After nondimensionalization, our toy problems all reduce to the same form:

$$\min_{h(x)} \left\{ \int_0^1 \left[ \frac{1}{h(x)} + h_x^2 \right] dx + \gamma h(0) + \gamma h(1) \right\}. \tag{6.1}$$

As explained in the preceding sections, the energy scaling laws follow from the following simple result:

**Lemma 6.1.** *For any $\gamma \gtrsim 1$, we have min* (6.1) $\sim 1$.

*Proof.* Let $e_{min}$ be the minimum value of (6.1) . The upper bound $e_{min} \lesssim 1$ is easy, requiring no condition on $\gamma$: It suffices to consider the test function

$$h(x) = \min\{x^{2/3}, (1 - x)^{2/3}\}.$$

For the lower bound, we assume $\gamma \geq c_0$ with $c_0 > 0$. Then obviously

$$h(0) \leq \frac{e_{min}}{c_0}.$$

But we also have, for any $0 \leq a < b \leq 1$,

$$\int_a^b \frac{1}{h} + h_x^2 \, dx \geq 2 \int_a^b \sqrt{\frac{1}{h}} \, |h_x| \, dx = 4 \int_a^b |(\sqrt{h})_x| \, dx \geq 4 \, |\sqrt{h(b)} - \sqrt{h(a)}|. \tag{6.2}$$

Now, if the optimal $h$ satisfies

$$h \leq \frac{2e_{min}}{c_0} \quad \text{uniformly on } [0, 1], \tag{6.3}$$

then

$$e_{min} \geq \int_0^1 \frac{1}{h} \, dx \geq \frac{c_0}{2e_{min}},$$

whence $e_{min} \geq \sqrt{c_0/2}$. Otherwise, if (6.3) is false, then (6.2) gives

$$e_{min} \geq 4\left[\left(\frac{2e_{min}}{c_0}\right)^{1/2} - \left(\frac{e_{min}}{c_0}\right)^{1/2}\right] = 4(\sqrt{2}-1)c_0^{-1/2}e_{min}^{1/2},$$

whence $e_{min} \geq Cc_0^{-1}$. Since both alternatives give lower bounds for $e_{min}$, the proof is complete. □

In the table below, we record the different predictions of $(\mathcal{TP})_{1-3}$ in two regimes for the relative size of the sample. The scaling "without branching" is obtained by restricting $h(x)$ to be constant (independent of $x$), while the scaling "with branching" is obtained by minimizing over all $h(x)$, assuming $\gamma_i \gtrsim 1$. The regime where branching is energetically preferable is determined by (a) direct comparison of the two scaling laws, or (equivalently) by (b) the condition that $\gamma_i \gtrsim 1$.

| Toy Problem / Structure | Minimum energy without branching | Minimum energy with branching | Branching regime |
|---|---|---|---|
| $(\mathcal{TP})_1$ 2D (n) threads cf. Sec. 4.1 | $b_a \lvert\log(b_a)\rvert^{1/2} \varepsilon^{1/2} L^{1/2}$ | $b_a^{1/3} \varepsilon^{2/3} L^{1/3}$ | $\varepsilon/L < b_a^4 \lvert\log(b_a)\rvert^3$ |
| $(\mathcal{TP})_1$ 2D (s) tunnels cf. Sec. 4.2 | $(1-b_a)\lvert\log(1-b_a)\rvert^{1/2} \varepsilon^{1/2} L^{1/2}$ | $(1-b_a)^{2/3} \varepsilon^{2/3} L^{1/3}$ | $\varepsilon/L < (1-b_a)^2 \lvert\log(1-b_a)\rvert^3$ |
| $(\mathcal{TP})_2$ 3D (n) treads cf. Sec. 4.3 | $b_a \varepsilon^{1/2} L^{1/2}$ | $b_a^{2/3} \varepsilon^{2/3} L^{1/3}$ | $\varepsilon/L < b_a^2$ |
| $(\mathcal{TP})_3$ 3D (s) tunnels cf. Sec. 4.4 | $(1-b_a) \varepsilon^{1/2} L^{1/2}$ | $(1-b_a) \lvert\log(1-b_a)\rvert^{1/3} \varepsilon^{2/3} L^{1/3}$ | $\varepsilon/L < \lvert\log(1-b_a)\rvert^{-2}$ |

## 7. Ansatz-Independent Bounds

This section addresses the issue of geometric complexity by proving ansatz-independent lower bounds. Our argument makes use of a well-known analogy between the intermediate state and micromagnetics. Briefly, we show that each superconducting domain pattern leads to an associated magnetization pattern (Section 7.1), then we use results from [11] to deduce the desired lower bounds (Section 7.2).

Our bounds and constructions have the same scaling law for intermediate values of $b_a$, but they differ by just a logarithmic factor for $b_a$ near 1. Moreover, they scale quite differently in the small-$b_a$ regime; for example, the bound has a prefactor of $b_a$, while the branched-normal-thread construction has a prefactor of $b_a^{2/3}$. The forthcoming paper [12] provides lower bounds with optimal scaling in $b_a$, $\varepsilon$, and $L$ for applied fields near 0 and 1. These results require a method different from the approach of this section—closer in spirit to that of Section 5.

### *7.1. A Connection with Micromagnetics*

For a uniaxial ferromagnet, the micromagnetics variational problem is the following: Among all unit vector fields $\mathbf{m}$ that vanish outside $\Omega \subset \mathbf{R^3}$, minimize

$$(\mathcal{M}) \qquad Q \int_\Omega m_2^2 + m_3^2 + \delta \int_\Omega |\nabla \mathbf{m}|^2 + \int_{\mathbf{R^3}} |\nabla u|^2,$$

where $\Delta u = \operatorname{div} \mathbf{m}$ in $\mathbf{R^3}$. Here $Q$ is the quality factor, measuring the "hardness" of the material, and $\delta$ is the exchange constant.

To focus on domain morphology without having to solve simultaneously for the internal structure of domain walls, it is natural to consider an analogous sharp-interface problem. This is common in the magnetics literature, where it goes by the name "domain theory" (see e.g. [35]). For a uniaxial ferromagnet, the natural problem is to minimize, among BV vector fields which vanish outside $\Omega$,

$$(\mathcal{M}_{\text{sharp}}) \qquad Q \int_\Omega m_2^2 + m_3^2 + \varepsilon \int_\Omega |\nabla \mathbf{m}| + \int_{\mathbf{R^3}} |\nabla u|^2.$$

Here $\Delta u = \operatorname{div} \mathbf{m}$ in $\mathbf{R^3}$ just as before, and $\epsilon$ denotes the surface tension of the domain walls. The correspondence between $(\mathcal{M})$ and $(\mathcal{M}_{\text{sharp}})$ is standard, and is discussed at length in [10].

We claim that $(\mathcal{M}_{\text{sharp}})$ is very closely related to our problem $(\mathcal{P})$. Indeed, if $\mathbf{B}$ and $\chi$ are test fields for $(\mathcal{P})$, consider the associated magnetization $\mathbf{m}$ defined by

$$\mathbf{m}(x, y, z) = (m_1(x, y, z), 0, 0) := \begin{cases} (-b_a, 0, 0) & \text{if } x \in [0, L] \text{ and } \chi = 1, \\ (1 - b_a, 0, 0) & \text{if } x \in [0, L] \text{ and } \chi = 0, \\ (0, 0, 0) & \text{if } x \notin [0, L]. \end{cases} \tag{7.4}$$

It is straightforward to see (see e.g. [10]) that the magnetic field $\nabla u$ equals $\pi_{\text{grad}}\mathbf{m}$, the $L^2$ projection of $\mathbf{m}$ onto the space of gradients. Hence setting $\widetilde{\mathbf{B}} = \mathbf{B} - (b_a, 0, 0)$, which is divergence-free, we have

$$\begin{aligned} \varepsilon \int_\Omega |\nabla m_1| + \left|\left|\pi_{\text{grad}}\mathbf{m}\right|\right|^2_{L^2(\mathbf{R^3})} &= \varepsilon \int_\Omega |\nabla m_1| + \left|\left|\pi_{\text{grad}}\left(\mathbf{m} - \widetilde{\mathbf{B}}\right)\right|\right|^2_{L^2(\mathbf{R^3})} \\ &\leq \varepsilon \int_\Omega |\nabla m_1| + \left|\left|\mathbf{m} - \widetilde{\mathbf{B}}\right|\right|^2_{L^2(\mathbf{R^3})}. \end{aligned} \tag{7.5}$$

One easily checks that the last line is precisely the energy associated with our problem $(\mathcal{P})$.

Our work [11] gave ansatz-independent lower bounds in the context of micromagnetics. Using (7.5), we also have ansatz-independent lower bounds on problem $(\mathcal{P})$. The remainder of Section 7 explains this observation and its consequences.

### *7.2. Patterns of Arbitrary Complexity, and Patterns of Arbitrary Complexity but Independent of $x$*

The following theorems are very close to the results in [11]. But we are interested in the scaling law of the prefactor as $b_a$ tends to 0 or 1, an issue not addressed in [11].

Therefore we repeat the (relatively short) proofs, for the reader's convenience.

**Theorem 7.1.** *Suppose*

$$\varepsilon/L \lesssim b_a^{3/2}\,(1-b_a)^{3/2} \qquad \text{and} \qquad \varepsilon^{1/3}\,L^{2/3} \lesssim 1. \tag{7.6}$$

*Then*

$$\min(\mathcal{P}) \gtrsim b_a\,(1-b_a)\,\epsilon^{2/3}\,L^{1/3}.$$

**Theorem 7.2.** *Suppose*

$$\varepsilon/L \lesssim b_a^2(1-b_a)^2 \qquad \text{and} \qquad \varepsilon^{1/2}\,L^{1/2} \lesssim 1. \tag{7.7}$$

*Then*

$$\min_{\chi,\ \mathbf{B}\ \textit{indep of}\ x} (\mathcal{P}) \gtrsim b_a\,(1-b_a)\,\varepsilon^{1/2}\,L^{1/2}.$$

*Proof of Theorem 7.1.* Suppose $\mathbf{B}$ and $\chi$ are admissible for $(\mathcal{P})$. We may assume without loss of generality that

$$\int_\Omega (1-\chi)(B_1-1)^2 \ < c_0\,b_a(1-b_a)\varepsilon^{2/3}\,L^{1/3}, \tag{7.8}$$

for any fixed $c_0$, since otherwise there is nothing to prove. The value of $c_0$ will be chosen in the course of the proof.

Consider the associated magnetization $\mathbf{m}$ defined by (7.4). It suffices to prove that

$$E(\mathbf{m}) := \big|\big|\pi_{\text{grad}}\mathbf{m}\big|\big|_{L^2}^2 + \varepsilon \int_\Omega |\,\nabla m_1\,| \gtrsim b_a\,(1-b_a)\,\varepsilon^{2/3}\,L^{1/3}.$$

Let $\widehat{\mathbf{m}}$ denote both the discrete Fourier series in $(y,z)\in Q$ and the Fourier transform in $x\in\mathbf{R}$, i.e.

$$\widehat{\mathbf{m}}(\xi,\mathbf{n}) = \int_{-\infty}^{\infty} e^{-2\pi i\xi x}\widehat{\mathbf{m}}(x,\mathbf{n})\,dx, \ \text{ with } \quad \widehat{\mathbf{m}}(x,\mathbf{n}) = \int_Q e^{-2\pi i(yn_1+zn_2)}\mathbf{m}(x,y,z)\,dy\,dz,$$

where $\mathbf{n}\in\mathbf{Z}^2$ and $\xi\in\mathbf{R}$. Notice that

$$\big|\big|\pi_{\text{grad}}\mathbf{m}\big|\big|_{L^2}^2 = \sum_{\mathbf{n}} \int_{-\infty}^{\infty} \frac{\xi^2}{\xi^2+|\mathbf{n}|^2}\,|\widehat{m}_1(\xi,\mathbf{n})|^2\,d\xi.$$

Using Lemma A.4 of the Appendix with $\lambda=|\mathbf{n}|$ and $g(x)=\widehat{m}_1(x,\mathbf{n})$, we have

$$\sum_{\mathbf{n}} \int_{-\infty}^{\infty} \frac{\xi^2}{\xi^2+|\mathbf{n}|^2}\,|\widehat{m}_1(\xi,\mathbf{n})|^2\,d\xi \gtrsim \int_0^L \sum_{\mathbf{n}} \frac{1}{1+(|\mathbf{n}|L)^2}\,|\widehat{m}_1(x,\mathbf{n})|^2\,dx.$$

Thus setting $\alpha := \max\{b_a, 1-b_a\} = ||m_1(x)||_{L^\infty(Q)} \geq \frac{1}{2}$, we have

$$
\begin{aligned}
&\varepsilon \int_\Omega |\nabla m_1| + \left|\left|\pi_{\text{grad}}\mathbf{m}\right|\right|_{L^2}^2 \\
&\quad \gtrsim \int_0^L \left\{ \varepsilon \int_Q |\nabla m_1(x,y,z)|\,dy\,dz + \sum_{\mathbf{n}} \frac{1}{1+(|\mathbf{n}|L)^2} |\widehat{m}_1(x,\mathbf{n})|^2 \right\} dx \\
&\quad \gtrsim \int_0^L \left(\frac{\varepsilon}{\alpha L}\right)^{2/3} \left\{ \left(\frac{\varepsilon L^2}{\alpha}\right)^{1/3} \alpha \int_Q |\nabla m_1(x)|\,dy\,dz \right. \\
&\qquad\qquad \left. + \left(\frac{\alpha L}{\varepsilon}\right)^{2/3} \sum_{\mathbf{n}} \min\left\{1, \frac{1}{(|\mathbf{n}|L)^2}\right\} |\widehat{m}_1(x,\mathbf{n})|^2 \right\} dx \\
&\quad \gtrsim \int_0^L \left(\frac{\varepsilon}{\alpha L}\right)^{2/3} \left\{ \left(\frac{\varepsilon L^2}{\alpha}\right)^{1/3} \alpha \int_Q |\nabla m_1(x)|\,dy\,dz \right. \\
&\qquad\qquad \left. + \sum_{\mathbf{n}} \min\left\{1, \frac{\alpha^{2/3}}{\varepsilon^{2/3} L^{4/3}} \frac{1}{|\mathbf{n}|^2}\right\} |\widehat{m}_1(x,\mathbf{n})|^2 \right\} dx \\
&\quad \gtrsim \left(\frac{\varepsilon}{L}\right)^{2/3} \int_0^L \int_Q m_1^2\,dx\,dy\,dz. \qquad (7.9)
\end{aligned}
$$

From line 3 to line 4 of (7.9), we made use of our hypothesis that $L \gtrsim \varepsilon$, and we passed from line 4 to line 5 by applying Lemma A.3(a) of the Appendix with the choice $N \cong \varepsilon^{-1/3} L^{-2/3} \alpha^{1/3}$, which is possible by the second inequality in (7.6) and the fact that $\alpha \geq \frac{1}{2}$.

Our final task is to relate $\int_0^L \int_Q m_1^2$ to $b_a$. We have

$$
\int_0^L \int_Q m_1^2\,dx\,dy\,dz = \int_0^L \int_Q b_a^2 \chi + (1-b_a)^2(1-\chi)\,dx\,dy\,dz. \qquad (7.10)
$$

Heuristically we expect $B_1 \approx 1-\chi$. If this relation held exactly, then matters would be easy: Using Lemma 3.1, the right-hand side of (7.10) would become $Lb_a(1-b_a)$. This together with (7.9) would give the desired estimate.

In general $B_1 \neq 1-\chi$, but the difference is controlled by (7.8). So we argue as follows: By Lemma 3.1,

$$
\begin{aligned}
&\int_0^L \int_Q b_a^2 \chi + (1-b_a)^2(1-\chi)\,dx\,dy\,dz \\
&= \int_0^L \int_Q (1-2b_a)(B_1 + 1 - \chi - B_1) + b_a^2\,dx\,dy\,dz \\
&= b_a(1-b_a)L + (1-2b_a) \int_0^L \int_Q 1 - \chi - B_1\,dx\,dy\,dz. \qquad (7.11)
\end{aligned}
$$

The condition $B_1\chi = 0$ implies $(1-\chi-B_1)^2 = (1-\chi)(B_1-1)^2$. Combining this with Hölders inequality, we have

$$\int_0^L \int_Q |1-\chi-B_1|\,dx\,dy\,dz \;\le\; L^{1/2}\left(\int_0^L\int_Q (1-\chi-B_1)^2\right)^{1/2} = L^{1/2}\left(\int_0^L\int_Q (1-\chi)(B_1-1)^2\right)^{1/2}.$$

Let $c_1$ be the constant implicit in the first part of (7.6):

$$\varepsilon/L \;\le\; c_1 b_a^{3/2}\,(1-b_a)^{3/2}.$$

Combining this relation and (7.8) with the preceding estimate, we get

$$\int_0^L \int_Q |1-\chi-B_1|\,dx\,dy\,dz \le c_0^{1/2} c_1^{1/3} b_a(1-b_a)L.$$

Choosing $c_0$ so that $c_0^{1/2}c_1^{1/3} \le 1/2$, we conclude from (7.11) that

$$\int_0^L \int_Q m_1^2\,dx\,dy\,dz \ge \frac{1}{2} b_a(1-b_a)L.$$

Combining this with (7.9) gives the desired estimate

$$E(\mathbf{m}) \;\gtrsim\; (\varepsilon/L)^{2/3}\; b_a\,(1-b_a)\,L. \qquad \square$$

*Proof of Theorem 7.2.* The argument is very similar, using part (b) of Lemma A.3 instead of part (a). The details can safely be left to the reader (see also [11]). $\square$

Theorems 7.1 and 7.2 show, roughly speaking, that

(a) there is no energetic incentive for in-plane complexity, and
(b) branching or refinement is required for energy minimization,

for intermediate applied fields and $\varepsilon/L \ll 1$. Indeed, for $b_a$ bounded away from 0 and 1, the minimum energy is of order $\varepsilon^{2/3}L^{1/3}$, and this scaling law is achieved by the highly ordered constructions of Section 4—even the laminar one of Section 4.1. Theorem 7.1 shows that no domain structure, regardless of its complexity, can achieve a better scaling law—this is the careful statement of point (a). And Theorem 7.2 shows that if branching and refinement were prohibited, the scaling law would be different, namely $\varepsilon^{1/2}L^{1/2} \gg \varepsilon^{2/3}L^{1/3}$—this is the careful statement of point (b).

We remark that the proof of our ansatz-independent lower bound shares some features with the constructions and toy problems. After renormalization of the total energy, i.e. factoring out $(\varepsilon/L)^{2/3}$, one must show that what remains is bounded below by a constant times the volume of the domain. The constructions are rather rigid; the assertion is true, but we wonder whether it is merely an accident. The toy problems are less rigid, fixing the geometry but optimizing over the local length scale $h(x)$; they show, in particular,

that the constructions' success is no accident. Theorem 7.1 is less rigid still, replacing the toy problem with an interpolation inequality; it shows that no as-yet-undiscovered construction can give a better scaling law.

The constructions and toy problems have one advantage over the ansatz-free viewpoint: They predict the local length scale *throughout* the plate. In the less rigid, ansatz-free setting, we are only able to estimate a suitably *averaged* length scale. This is explained in Section 7.3.

### *7.3. Average Domain Width of Minimizing Structures*

We have focused on the scaling law of the minimum energy. In truth, however, the experimentally relevant scaling law is not that of the minimum energy, but rather that of the microstructural length scale. Indeed, the length scale is readily observable (especially at the faces of the plate). Such measurements—combined with a theoretical scaling law—represent the principal means for estimating the surface tension $\varepsilon$ of the superconductor-normal interface.

Traditionally, the scaling law for the microstructural length scale has been deduced by considering constructions like those of Section 4. Our "toy problems" could provide an attractive alternative, but we shall not pursue this here. Rather, we wish to explain how Theorem 7.1 yields ansatz-free upper and lower bounds for the *average* length scale—more precisely, for the total perimeter per unit volume.

For any $\mathbf{B}$ and $\chi$ admissible for problem $(\mathcal{P})$, let

$$\mathcal{D}(\mathbf{B}, \chi) = \frac{\text{volume of } \Omega}{\text{total surface area}} = \frac{L}{\int_\Omega |\nabla \chi|}.$$

Clearly $\mathcal{D}(\mathbf{B}, \chi)$ has dimensions of length; for dyadically branched constructions like those of Section 4 it is (a constant times) the length scale in the middle of the plate. So we view $\mathcal{D}(\mathbf{B}, \chi)$ as an ansatz-free, global measure of the microstructural length scale.

**Theorem 7.3.** *For any $\delta > 0$, and any $0 < b_a < 1$, there exist constants $C_1$, $C_2$, $C_3$, and $C_4$ (depending on $\delta$ and $b_a$) such that*

$$\varepsilon/L \le C_1 \qquad \text{and} \qquad \varepsilon^{1/3} L^{2/3} \le C_1$$

*imply*

*(a)* $\min(\mathcal{P}) \le C_2 \varepsilon^{2/3} L^{1/3}$, *and*
*(b) if* $\mathbf{B}$ *and* $\chi$ *are admissible for* $(\mathcal{P})$ *and achieve value* $\le \frac{1}{\delta} C_2 \varepsilon^{2/3} L^{1/3}$, *then*

$$C_3 \varepsilon^{1/3} L^{2/3} \le \mathcal{D}(\mathbf{B}, \chi) \le C_4 \varepsilon^{1/3} L^{2/3}.$$

Thus the energy-minimizing domain pattern has length scale of order $\varepsilon^{1/3} L^{2/3}$—and so does any pattern that comes within a factor of $1/\delta$ of the minimum value.

*Proof.* The argument is identical to that of Proposition 4.1 in [11]. Therefore we just indicate the main idea. Theorem 7.1 with $\varepsilon$ replaced by $M\varepsilon$ gives

$$C(b_a)(M\varepsilon)^{2/3} L^{1/3} \le (M\varepsilon) \int_\Omega |\nabla \chi| + \int_\Omega B_2^2 + B_3^2 + (1-\chi) B_1^2 + \int_{\Omega^c} |\mathbf{B} - \mathbf{b_a}|^2,$$

while by hypothesis we have

$$\frac{1}{\delta}C_2\varepsilon^{2/3}L^{1/3} \;\geq\; \varepsilon\int_\Omega |\nabla\chi| \;+\; \int_\Omega B_2^2 + B_3^2 + (1-\chi)B_1^2 \;+\; \int_{\Omega^c} |\mathbf{B}-\mathbf{b_a}|^2.$$

If $M$ is sufficiently large, then we may subtract the latter from the former to deduce an estimate of the form

$$\varepsilon\int_\Omega |\nabla\chi| \;\geq\; C\varepsilon^{2/3}L^{1/3},$$

which can be rewritten as $\mathcal{D}(\mathbf{B},\,\chi) \leq C_4\varepsilon^{1/3}L^{2/3}$. The opposite inequality is trivial: Since the magnetic terms are nonnegative, we have $\varepsilon\int_\Omega |\nabla\chi| \;\leq\; \frac{1}{\delta}C_2\varepsilon^{2/3}L^{1/3}$, which can be rewritten as $\mathcal{D}(\mathbf{B},\,\chi) \geq C_3\varepsilon^{1/3}L^{2/3}$. □

The same method can be applied to domain patterns that are independent of $x$. This restriction changes the scaling law to

$$C_3\varepsilon^{1/2}L^{1/2} \;\leq\; \mathcal{D}(\mathbf{B},\,\chi) \;\leq\; C_4\varepsilon^{1/2}L^{1/2},$$

and the proof naturally uses Theorem 7.2 rather than Theorem 7.1.

It would be interesting to obtain a pointwise estimate of the length scale—e.g. to prove it is correctly predicted by the appropriate toy problem from Section 6. To prove such a result, one would surely have to use additional information beyond simply assuming the energy is small. Our Theorem 7.3 makes no use of any optimality condition; but it is natural to expect that more should be true at (local or global) minima. See [13], [30] for results of this type in a related but different setting.

## 8. Conclusion

The analysis of the intermediate state is at once a topic in the calculus of variations and a problem of energy-driven pattern formation. The variational viewpoint is convenient because it permits us to ask—and in large measure answer—a precise question: What is the scaling law of the minimum energy? The answer is interesting due to its unexpected complexity near $b_a = 0$ and $b_a = 1$. The analysis is interesting as well, since it involves ansatz-independent lower bounds.

In the end, however, we are interested in the patterns, not the energy scaling law. We want to understand what robust features are shared by all patterns with a given energy scaling. The usual approach to this question is to examine alternative constructions. Our toy problems and bounds are valuable because they offer additional, rather different insight.

From our perspective, the analysis of the intermediate state is the study of a particular nonconvex variational problem regularized by surface energy. There is, at present, no general method for identifying optimal scaling laws and patterns for such problems. The route to a general understanding is surely by way of examples like this one.

## A. Appendix

This appendix discusses the relevant properties of the space $H^{-1/2}$ and recalls two lemmas from [11]. Let $L^2_\sharp$ be the space of $Q$-periodic $L^2$ functions with mean value 0 (recall that $Q = [0, 1]^2$). The subspace $H^{-1/2}(Q) \subset L^2_\sharp\mathcal{L}$ is defined as

$$H^{-1/2}(Q) \;=\; \left\{ f \in L^2_\sharp \;\middle|\; \sum_{|\mathbf{n}|\neq 0} \frac{|\widehat{f}(\mathbf{n})|^2}{|\mathbf{n}|} \;<\; \infty \right\},$$

and we define

$$\|f\|^2_{H^{-1/2}(Q)} \;=\; \sum_{|\mathbf{n}|\neq 0} \frac{|\widehat{f}(\mathbf{n})|^2}{|\mathbf{n}|}.$$

Here $\mathbf{n} \in \mathbf{Z}^2$, and $\widehat{f}(\mathbf{n})$ denotes the $\mathbf{n}$th Fourier coefficient of $f$. The following proposition explains why the external magnetic field energy is estimated by the $H^{-1/2}$ norm of $B_1 - b_a$ evaluated at $x = 0$ and $x = L$.

**Proposition A.1.** *Let $f \in H^{-1/2}(Q)$ and consider the unique finite energy solution (periodic in $y$ and $z$) to the Neumann problem*

$$\Delta u \;=\; 0 \quad \text{in } [0,\infty)\times Q \quad \textit{with} \quad u_x(0, y, z) \;=\; f.$$

*Then*

$$\int_{[0,\infty)\times Q} |\nabla u|^2 \, dx\, dy\, dz \;=\; \frac{1}{2\pi}\, \|f\|^2_{H^{-1/2}(Q)}.$$

*Proof.* Denoting the discrete Fourier transform of $u(x, y, z)$ in the $y$ and $z$ variables by $\widehat{u}(x, \mathbf{n})$ with $\mathbf{n} = (n_1, n_2) \in \mathbf{Z}^2$, we have

$$u(x, y, z) \;=\; \sum_{|\mathbf{n}|\neq 0} \widehat{u}(x, \mathbf{n})\, e^{2\pi i (n_1 y + n_2 z)}.$$

Thus

$$\widehat{u}(x, \mathbf{n})_{xx} \;-\; (2\pi|\mathbf{n}|)^2 \widehat{u}(x, \mathbf{n}) \;=\; 0, \qquad \widehat{u}(0, \mathbf{n})_x \;=\; \widehat{f}(\mathbf{n}).$$

Hence,

$$\widehat{u}(x, \mathbf{n}) \;=\; -e^{-2\pi|\mathbf{n}|x}\, \frac{\widehat{f}(\mathbf{n})}{2\pi|\mathbf{n}|},$$

and

$$\begin{aligned}\int_0^\infty \int_Q |\nabla u|^2 \, dy\, dz\, dx \;&=\; \sum_{|\mathbf{n}|\neq 0} \int_0^\infty 2e^{-4\pi|\mathbf{n}|x} |\widehat{f}(\mathbf{n})|^2 \, dx \\ &=\; \sum_{|\mathbf{n}|\neq 0} \frac{|\widehat{f}(\mathbf{n})|^2}{2\pi|\mathbf{n}|} \;=\; \frac{1}{2\pi}\, \|f\|^2_{H^{-1/2}(Q)}.\end{aligned}$$

□

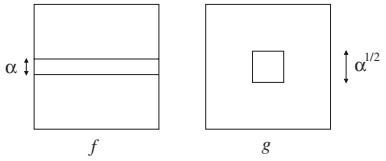


**Fig. 10.**

For the constructions in Section 4, $B_1$ is piecewise constant and periodic in $y$ and $z$. The next proposition estimates the $H^{-1/2}$ norms of such functions. For $\alpha \in (0, \frac{1}{2})$, consider $f, g \in L^2_\sharp$ defined as follows (see Figure 10):

$$f(y,z) := \begin{cases} 1-\alpha & \text{if } \frac{1-\alpha}{2} < z < \frac{1+\alpha}{2}, \\ -\alpha & \text{otherwise,} \end{cases}$$

$$g(y,z) := \begin{cases} 1-\alpha & \text{if } \frac{1-\sqrt{\alpha}}{2} < y, z < \frac{1+\sqrt{\alpha}}{2}, \\ -\alpha & \text{otherwise.} \end{cases}$$

**Proposition A.2.** *Extend both $f$ and $g$ to $\mathbf{R}^2$ by periodicity, and for any natural number $m$, define $f_m(y,z) := f(y,mz)$ and $g_m(y,z) := g(my,mz)$. They satisfy*

$$\|f_m\|^2_{H^{-1/2}(Q)} \lesssim \frac{\alpha^2\,|\log(\alpha)|}{m} \qquad \text{and} \qquad \|g_m\|^2_{H^{-1/2}(Q)} \lesssim \frac{\alpha^{3/2}}{m}.$$

*Proof.* From the definition of the Fourier coefficients, it is straightforward to check that

$$\|f_m\|^2_{H^{-1/2}(Q)} = \frac{1}{m}\,\|f\|^2_{H^{-1/2}(Q)} \qquad \text{and} \qquad \|g_m\|^2_{H^{-1/2}(Q)} = \frac{1}{m}\,\|g\|^2_{H^{-1/2}(Q)}.$$

Since we are only concerned with $\widehat{g}(\mathbf{n})$ and $\widehat{f}(\mathbf{n})$ for $\mathbf{n} \neq 0$, it suffices to consider $(\widehat{g+\alpha})(\mathbf{n})$ and $(\widehat{f+\alpha})(\mathbf{n})$. Focusing first on $g$, we have (by a convenient translation within $Q$)

$$\begin{aligned} |(\widehat{g+\alpha})(\mathbf{n})|^2 &\cong \left|\int_0^{\alpha^{1/2}} e^{2\pi i n_1 y}\,dy\right|^2 \left|\int_0^{\alpha^{1/2}} e^{2\pi i n_2 z}\,dz\right|^2 \\ &= \frac{1}{n_1^2}\left|e^{2\pi i n_1 \alpha^{1/2}} - 1\right|^2 \frac{1}{n_2^2}\left|e^{2\pi i n_2 \alpha^{1/2}} - 1\right|^2 \\ &\lesssim \frac{\alpha}{1+\alpha n_1^2}\,\frac{\alpha}{1+\alpha n_2^2}. \end{aligned}$$

Therefore,

$$\begin{aligned} \|g\|^2_{H^{-1/2}(Q)} = \sum_{|\mathbf{n}|\neq 0} \frac{|\widehat{g}(\mathbf{n})|^2}{|\mathbf{n}|} &\lesssim \sum_{|\mathbf{n}|\neq 0} \frac{1}{|\mathbf{n}|}\,\frac{\alpha}{1+\alpha n_1^2}\,\frac{\alpha}{1+\alpha n_2^2} \\ &\lesssim \int_0^\infty \int_0^\infty \frac{1}{\sqrt{y^2+z^2}}\,\frac{\alpha}{1+\alpha y^2}\,\frac{\alpha}{1+\alpha z^2}\,dy\,dz \end{aligned}$$

$$\lesssim \alpha^{3/2} \int_0^\infty \int_0^\infty \frac{1}{\sqrt{y^2+z^2}} \frac{1}{1+y^2} \frac{1}{1+z^2}\, dy\, dz$$
$$\lesssim \alpha^{3/2}.$$

The analysis of $f$ is similar:

$$\|f\|^2_{H^{-1/2}(Q)} = \sum_{|\mathbf{n}|\neq 0} \frac{|\widehat{f}(\mathbf{n})|^2}{|\mathbf{n}|} \lesssim \int_1^\infty \frac{1}{z} \frac{\alpha^2}{1+\alpha^2 z^2}\, dz$$
$$\lesssim \alpha^2 \int_\alpha^\infty \frac{1}{z} \frac{1}{1+z^2}\, dz$$
$$\lesssim \alpha^2 |\log(\alpha)|. \qquad \square$$

Finally we state two lemmas proved in [11].

**Lemma A.3.** *For any $Q$-periodic function $f$, and any positive integer $N$,*

$$(a) \quad \int_Q |f|^2\, dx\, dy \lesssim \left\{ \frac{1}{N} \sup_Q |f| \int_Q |\nabla f|\, dx\, dy + \sum_{\mathbf{n}\in\mathbf{Z}^2} \min\left\{1, \frac{N^2}{|\mathbf{n}|^2}\right\} |\widehat{f}(\mathbf{n})|^2 \right\}, \tag{A.1}$$

*and*

$$(b) \quad \int_Q |f|^2\, dx\, dy \lesssim \left\{ \frac{1}{N} \sup_Q |f| \int_Q |\nabla f|\, dx\, dy + \sum_{\mathbf{n}\in\mathbf{Z}^2} \min\left\{1, \frac{N}{|\mathbf{n}|}\right\} |\widehat{f}(\mathbf{n})|^2 \right\}. \tag{A.2}$$

**Lemma A.4.** *Consider any $g : \mathbf{R} \to \mathbf{R}$ such that $g(x) = 0$ for $|x| > L$. Then for any $\lambda \in \mathbf{R}$,*

$$\int_{-\infty}^\infty \frac{\xi^2}{\xi^2+\lambda^2} |\widehat{g}(\xi)|^2\, d\xi \gtrsim \frac{1}{1+(\lambda L)^2} \int_{-L}^L |g(x)|^2\, dx.$$

## References


[1] Andrews, E.R. The intermediate state of superconductors III. Theory of behavior of superconducting cylinders in transverse magnetic fields. *Proc. Roy. Soc. London* A **194**, 98–112 (1948).

[2] Balashova, B.M., and Sharvin, I.V. Structure of the intermediate state of superconductors. *Sov. Phys. JETP* **4** no. 1, 54–59 (1957).

[3] Ben Belgacem, H., Conti, S., DeSimone, A., Müller, S. Rigorous bounds for the Föppl–von Karman theory of isotropically compressed plates. *J. Nonlinear Sci.* **10**, 661–683 (2000).

[4] Bhattacharya, K., Firoozye, N., James, R.D., and Kohn, R.V. Restrictions on microstructure. *Proc. Roy. Soc. Edinburgh* Sect. A **124**, 843–878 (1994).

[5] Bronsard, L., and Stoth, B. The Ginzburg-Landau equations of superconductivity and the one-phase Stefan problem. *Annales l' Institute Henri Poincare—Analyse Non Lineaire* **15**, 371–397 (1998).

[6] Chapman, S.J. Asymptotic analysis of the Ginzburg-Landau model of superconductivity: Reduction to a free boundary model. *Quart. Appl. Math.* **LIII-4**, 601–627 (1995).

[7] Chapman, S.J., Howison, S.D., Mcleod, J.B., and Ockendon, J.R. Normal/superconducting transitions in the Landau-Ginzburg theory. *Proc. Roy. Soc. Edinburgh Sect. A* **119**, 117–124 (1991).
[8] Chapman, S.J., Howison, S.D., and Ockendon, J.R. Macroscopic models for superconductivity. *SIAM Rev.* **34**, 529–560 (1992).
[9] Choksi, R. Scaling laws in microphase separation of diblock copolymers. *J. Nonlinear Sci.* **11**, 223–236 (2001).
[10] Choksi, R., and Kohn, R.V. Bounds on the micromagnetic energy of a uniaxial ferromagnet. *Commun. Pure Appl. Math.* **51**, 259–289 (1998).
[11] Choksi, R., Kohn, R.V., and Otto, F. Domain branching in uniaxial ferromagnets: A scaling law for the minimum energy. *Commun. Math. Phys.* **201**, 61–79 (1999).
[12] Choksi, R., Conti, S., Kohn, R.V., and Otto, F. In preparation.
[13] Conti, S. Branched microstructures: Scaling and asymptotic self-similarity. *Commun. Pure Appl. Math.* **53**, 1448–1474 (2000).
[14] Dacorogna, B. *Direct Methods in the Calculus of Variations*. Springer-Verlag, New-York, (1989).
[15] Dorsey, A.T., and Goldstein, R.E. The shape of flux domains in the intermediate state of type-I superconductors. *Phys. Rev.* B **57**, 3058–3072 (1998).
[16] Dzyaloshinskii, I.E. *Dokl. Akad. Nauk SSSR* **105**, 244 (1955).
[17] Evans, L.C., and Gariepy, R.F. *Measure Theory and Fine Properties of Functions*. CRC Press (1992).
[18] Faber, T.E. The intermediate state in superconducting plates. *Proc. Roy. Soc. London* A **248**, 460–481 (1958).
[19] Goldstein, R.E., Jackson, D.P., and Dorsey, A.T. Current-loop model for the intermediate state of type-I superconductors. *Phys. Rev. Lett.* **76**, 3818–3821 (1996).
[20] Haenssler, Fr., and Rinderer, L. Topologie de la structure de l'etat intermédiaire des supraconducteurs du type I et mesure de l'energie de surface. *Helv. Phys. Acta* **38**, 448–454 (1965).
[21] Hubert, A. Zur theorie der zweiphasigen domänenstrufturen in supraleitern und ferromagneten, *Phy. Stat. Sol.* **24**, 669–682 (1967).
[22] Hubert, A., and Schäfer, R. *Magnetic Domains*, Springer-Verlag, New-York (1998).
[23] Huebener, R.P. *Magnetic Flux Structures in Superconductors*. Springer-Verlag, New-York (1979).
[24] James, R., and Kinderlehrer, D. Frustration in ferromagnetic materials. *Cont. Mech. Thermodyn.* **2**, 215–239 (1990).
[25] Jin, W., and Kohn, R.V. Singular perturbation and the energy of folds. *J. Nonlinear Sci.* **10**, 355–390 (2000).
[26] Jin, W., and Sternberg, P. Energy estimates for the von Karman model of thin-film blistering. *J. Math. Phys.* **42**, 192–199 (2001).
[27] Kohn, R.V. The relaxation of a double-well energy. *Cont. Mech. Thermodyn.* **3**, 193–236 (1991).
[28] Kohn, R.V., and Müller, S. Branching of twins near an austenite twinned-martensite interface. *Phil. Mag.* A **66**, 697–715 (1992).
[29] Kohn, R.V., and Müller, S. Relaxation and regularization of nonconvex variational problems. *Rend. Sem. Mat. Fis. Univ. Milano* **62**, 89–113 (1992).
[30] Kohn, R.V., and Müller, S. Surface energy and microstructure in coherent phase transitions. *Commun. Pure Appl. Math.* **47**, 405–435 (1994).
[31] Kohn, R.V., and Otto, F. Small surface energy, coarse graining, and selection of microstructure. *Physica D* **107**, 272–289 (1997).
[32] Kohn, R.V., and Strang, G. Optimal design and relaxation of variational problems I–III. *Commun. Pure Appl. Math.* **39**, 113–137 (I), 139–182 (II), 353–377 (III) (1986).
[33] Landau, L. D. *Sov. Phys. JETP* **7**, (1937).
[34] Landau, L. D. On the theory of the intermediate state of superconductors. *J. Phys. U.S.S.R.* **7**, 99 (1943).

[35] Landau, L.D., and Lifshitz, E.M. *Electrodynamics of Continuous Media.* Addison-Wesley, Reading, MA (1960).
[36] Lifshitz, E.M., and Sharvin, I.V. *Dokl. Akad. Nauk SSSR* **79**, 783 (1951).
[37] Livingston, J.D., and DeSorbo, W. The intermediate state in type I superconductors. In *Superconductivity II*, ed. R.D. Parks, M. Dekker, New York (1969), 1235–1281.
[38] Nishiura, Y., and Ohnishi, I. Some mathematical aspects of the micro-phase separation in diblock copolymers. *Physica D* **84**, 31–39 (1995).
[39] Privorotskii, I. *Thermodynamic Theory of Domain Structures*. John Wiley & Sons, New York (1976).
[40] Reisin, C.R., and Lipson, S.G. Intermediate-state structures of type-I superconductors. *Phys. Rev. B* **61**, 4251–4258 (2000).
[41] Ren, X., and Wei, J. Energy minimizers for the diblock copolymer problem. *Interfaces Free Bound*. **5**, 193–238 (2003).
[42] Sharvin, I.V. Measurement of the surface tension at the boundary between superconducting and normal phases. *Soviet Phys. JETP* **6**, 1031 (1958).
[43] Tinkham, M. *Introduction to Superconductivity*. McGraw Hill, New York (1996).